



# A Lorenz-type attractor in a piecewise-smooth system: Rigorous results

Cite as: Chaos **29**, 103108 (2019); <https://doi.org/10.1063/1.5115789>

Submitted: 19 June 2019 . Accepted: 13 September 2019 . Published Online: 08 October 2019

Vladimir N. Belykh, Nikita V. Barabash , and Igor V. Belykh 

## COLLECTIONS

 This paper was selected as an Editor's Pick



[View Online](#)



[Export Citation](#)



[CrossMark](#)

**Scilight** Highlights of the best new research  
in the **physical sciences**

[LEARN MORE!](#)



# A Lorenz-type attractor in a piecewise-smooth system: Rigorous results

Cite as: Chaos 29, 103108 (2019); doi: 10.1063/1.5115789

Submitted: 19 June 2019 · Accepted: 13 September 2019 ·

Published Online: 8 October 2019



View Online



Export Citation



CrossMark

Vladimir N. Belykh,<sup>1,2,a)</sup> Nikita V. Barabash,<sup>1,2,b)</sup>  and Igor V. Belykh<sup>3,c)</sup> 

## AFFILIATIONS

<sup>1</sup>Department of Mathematics, Volga University of Water Transport, 5A, Nesterov str., Nizhny Novgorod 603950, Russia

<sup>2</sup>Department of Control Theory, Lobachevsky State University of Nizhny Novgorod, 23, Gagarin Ave., 603950 Nizhny Novgorod, Russia

<sup>3</sup>Department of Mathematics and Statistics, Georgia State University, P.O. Box 4110, Atlanta, Georgia 30302-410, USA

<sup>a)</sup>Electronic mail: [belykh@unn.ru](mailto:belykh@unn.ru)

<sup>b)</sup>Electronic mail: [barabash@itmm.unn.ru](mailto:barabash@itmm.unn.ru)

<sup>c)</sup>Author to whom correspondence should be addressed: [ibelykh@gsu.edu](mailto:ibelykh@gsu.edu)

## ABSTRACT

Chaotic attractors appear in various physical and biological models; however, rigorous proofs of their existence and bifurcations are rare. In this paper, we construct a simple piecewise-smooth model which switches between three three-dimensional linear systems that yield a singular hyperbolic attractor whose structure and bifurcations are similar to those of the celebrated Lorenz attractor. Due to integrability of the linear systems composing the model, we derive a Poincaré return map to rigorously prove the existence of the Lorenz-type attractor and explicitly characterize bifurcations that lead to its birth, structural changes, and disappearance. In particular, we analytically calculate a bifurcation curve explicit in the model's parameters that corresponds to the formation of homoclinic orbits of a saddle, often referred to as a “homoclinic butterfly.” We explicitly indicate the system's parameters that yield a bifurcation of two heteroclinic orbits connecting the saddle fixed point and two symmetrical saddle periodic orbits that gives birth to the chaotic attractor as in the Lorenz system. These analytical tasks are out of reach for the original nonintegrable Lorenz system. Our approach to designing piecewise-smooth dynamical systems with a predefined chaotic attractor and exact solutions may open the door to the synthesis and rigorous analysis of hyperbolic attractors.

Published under license by AIP Publishing. <https://doi.org/10.1063/1.5115789>

Does the Lorenz attractor exist? Although the Lorenz attractor<sup>1</sup> is an icon of chaos theory and has held that title since 1963, it was not until 1999 that the question of its existence was answered in the affirmative via a rigorous computer-assisted proof.<sup>2,3</sup> Obstacles to proving the existence of a chaotic attractor in a nonlinear system of ordinary differential equations (ODEs) include one's inability to obtain exact solutions due to nonintegrability of the underlying dynamical system. To avoid this obstacle, we propose an elegant geometrical method of synthesizing a piecewise-smooth ODE system that can switch between several linear systems with known exact solutions that can display a chaotic attractor whose structure and bifurcations can be described rigorously without any computer assistance. This strange chaotic attractor resembles the Lorenz attractor and has similar bifurcation properties. We analytically construct a Poincaré return map to characterize a bifurcation sequence that causes the emergence and disappearance of the chaotic attractor and calculate the corresponding

bifurcation curves expressed explicitly via the system's parameters. We also rigorously prove that one of the Lyapunov exponents of each trajectory comprising the attractor is positive, thereby demonstrating its chaoticity. Our geometrical approach promises to allow for constructing analytically tractable piecewise-smooth dynamical systems that can reproduce main properties of other known attractors, including the Rössler attractor that is notoriously known for its resistance to analytical studies.

## I. INTRODUCTION

The classical Lorenz attractor<sup>1</sup> has been the symbol of chaotic dynamics for more than 50 years. The discovery of the Lorenz attractor led to formulating a general concept of a strange attractor<sup>4</sup> which, in simple words,<sup>5</sup> is an attracting, invariant limit set composed of only unstable trajectories.

The Lorenz system and its extensions were studied in detail through geometrical models<sup>6–14</sup> by constructing discrete-time maps that model the behavior of flow-generated Poincaré return maps. Rigorous studies of the geometrical models revealed major bifurcational properties of the Lorenz attractor that were also confirmed via numerical simulations. These properties include bifurcational routes to the birth of the strange chaotic attractor in the Lorenz system such as (i) the major route (COD1) through a codimension-one bifurcation that involves the formation of two heteroclinic orbits of the saddle fixed point that connect to two symmetric saddle periodic orbits<sup>7,8</sup> and (ii) a codimension-two bifurcation route (COD2) through a codimension-two bifurcation of a homoclinic butterfly with a zero saddle value.<sup>11–13</sup> Other details of the fine bifurcation structure of the Lorenz system associated with the birth, evolution, and disappearance of the Lorenz attractor were studied through computer-assisted and numerical methods.<sup>7,15–25</sup> This body of work includes a detailed computational analysis of the existence of infinitely many periodic orbits with specific symbolic signatures related to homoclinic and heteroclinic bifurcations involving intersections with the stable manifold of the saddle fixed point.<sup>15,18,20</sup> A computer-assisted proof of the existence of the chaotic Lorenz attractor was recently given in Ref. 2. More specifically, this computer proof relied on interval-arithmetic techniques for estimating the computational errors and demonstrated that the Lorenz system has a chaotic attractor in a small neighborhood of the classical parameter values.<sup>15</sup> Earlier computer proofs of the existence of chaotic (not necessarily attracting) dynamics in the Lorenz system used a shooting method<sup>21</sup> and the demonstration of the existence of a horseshoe in the flow-defined Poincaré map<sup>22</sup> and positive topological entropy.<sup>24</sup>

Extending earlier results<sup>11–13</sup> related to the codimension-two bifurcation route COD2, an analytical (free of computer assistance) proof of the Lorenz attractor existence in an extended Lorenz system was presented in Ref. 26. This proof relied on the verification of the Shilnikov criteria<sup>27</sup> on the birth of a strange attractor and was based on the study of a small vicinity of a codimension-two bifurcation point, which corresponds to the homoclinic butterfly with a zero saddle value and, therefore, requires a simultaneous change of two parameters to reach it. These results represent significant progress in completely rigorous studies of the Lorenz system and its extension. However, a rigorous analytical study of the emergence of the Lorenz attractor through the codimension-one heteroclinic bifurcation via the main route COD1 seems elusive. Such a study would require analytically finding these heteroclinic orbits in the original Lorenz system to explicitly identify the corresponding system parameters. This study is associated with many technical difficulties due to nonintegrability of the nonlinear Lorenz system and, therefore, remains out of reach. However, rigorous computer-assisted methods,<sup>28</sup> including *a priori* bootstrap,<sup>23</sup> yielded a parameter-dependent study of the Lorenz system and validated heteroclinic connections related to the main bifurcation route COD1. Similarly, while a rigorous analytical proof<sup>29</sup> of a homoclinic bifurcation (the homoclinic butterfly) in the Lorenz system dates back to 1984, determining explicit parameters under which the bifurcation occurs in the Lorenz system is only possible via computer-assisted methods.<sup>25</sup>

In this paper, we address these problems in a different setting where we replace the original Lorenz system with a piecewise-smooth ODE system, which switches between three linear systems and whose

structure and chaotic attractor are similar to those of the Lorenz system. As trajectories of the piecewise-smooth systems are “glued” from trajectories of the linear systems, we are able to rigorously prove the existence of a strange attractor and explicitly indicate the system’s parameters that correspond to the codimension-one heteroclinic bifurcation and the main route COD1 as in the Lorenz system.

Piecewise-linear and piecewise-smooth systems were widely used in dynamical systems theory in different contexts and applications.<sup>30–33</sup> Their potential advantage over their nonlinear counterparts is the ability to derive explicit solutions in some partitions of a system’s phase space and “glue” the solutions at the partitions’ boundaries. Traditionally, piecewise-linear dynamical systems are derived from nonlinear dynamical systems by replacing nonlinearities with piecewise-linear functions to replicate the dynamics of a given nonlinear system and simplify its analysis. The classical example of such a replacement is the seminal work by Levinson<sup>34</sup> that targeted the dynamics of the driven Van der Pol equation where the term  $(x^2 - 1)$  was approximated by a piecewise constant function.<sup>34</sup> The use of the piecewise-linear system allowed Levinson to provide a rigorous basis for the classical result by Cartwright and Littlewood on the emergence of a complicated set of periodic orbits in the driven Van der Pol equation,<sup>35</sup> which is largely viewed as a first example of a deterministic system with possible chaotic behavior.

Piecewise-linear systems were also used to approximate and model the dynamics of the Lorenz system. Examples include a Lorenz-type piecewise-linear system<sup>36</sup> and a partial and complete linearized version of the Lorenz system<sup>37</sup> which were proposed to simplify chaotic circuit implementations for potential engineering and physics applications of chaos. Yet, no rigorous insights into the bifurcation structure of the piecewise-linear Lorenz systems were given.

Another large class of dynamical systems is piecewise-smooth dynamical systems<sup>30,31,38</sup> widely used in engineering as relay, automatic control, and switching systems.<sup>39–42</sup> An important example of such a piecewise-smooth system is a model of human gait,<sup>43</sup> which switches between two potentially linear systems<sup>44</sup> when a walker switches from one leg to the other. As a result, the trajectory of the piecewise-smooth system is composed of two linear solutions, thereby allowing one to derive exact forms of the walker’s periodic motion.<sup>45</sup>

In this work, we exploit the simplicity of piecewise-smooth dynamical systems toward developing a new approach to constructing analytically tractable piecewise-smooth dynamical systems that can reproduce main properties of a chaotic nonlinear system and facilitate its rigorous analysis. Our approach is motivated by the following logic. Suppose that a bifurcation structure of a chaotic attractor in a nonlinear, nonintegrable system, be it the Lorenz, Chua,<sup>46</sup> or Rössler<sup>47</sup> system, is known to a certain degree from direct numerical simulations. Can one construct a piecewise-smooth system for which it is possible to rigorously describe both the structure of the chaotic attractor and explicitly identify bifurcation routes to its emergence and disappearance that match the numerically revealed properties of the original nonlinear system?

This work provides a positive answer to this question and introduces a simple piecewise-smooth model which switches between three three-dimensional linear systems that yield a singular

hyperbolic attractor whose structure and bifurcations are similar to those of the Lorenz attractor. Due to integrability of the linear systems composing the model, we derive an exact Poincaré return map to rigorously prove the existence of a chaotic Lorenz-type attractor and characterize the two bifurcation routes COD1 and COD2 to the birth of the strange attractor explicit in the system's parameters. Using the explicit Poincaré return map, we prove that a Lyapunov exponent of each trajectory composing the attractor is positive and demonstrate that the attractor is chaotic and belongs to the class of the Lorenz-type singular hyperbolic attractors.<sup>48–50</sup> Note that in contrast to the classical hyperbolic attractors such as Anosov diffeomorphisms<sup>51</sup> and Smale-Williams solenoids,<sup>52</sup> which are chaotic and structurally stable, Lorenz-type attractors undergo a countable number of multiloop homoclinic bifurcations at which the attractors become structurally unstable and, therefore, are called singular hyperbolic.

Our approach is not limited to the Lorenz system, but rather applicable to other chaotic ODE systems whose bifurcation structure, chaoticity, and hyperbolicity are yet to be described rigorously. Strange hyperbolic attractors are hard to find in real physical systems described by ODEs. Several candidates of such nonlinear ODE systems with the Plykin attractor<sup>53,54</sup> and the Smale-Williams solenoids<sup>55,56</sup> were identified. A numerical analysis of these attractors gave a convincing argument in favor of their hyperbolicity;<sup>56</sup> yet, a rigorous proof is still missing. In light of this, our approach to designing piecewise-smooth dynamical systems with a predefined chaotic attractor and explicit solutions may open the door to the synthesis and an analytical proof of hyperbolic chaos in such systems. This approach complements our previous study<sup>57</sup> which suggested a way of embedding a singular hyperbolic attractor of a 2D map with singularities (the Belykh map) into the 3D phase space of a piecewise-smooth ODE system. This ODE system possesses a singular hyperbolic attractor whose chaotic and ergodic properties can be rigorously proved.<sup>58</sup>

The layout of this paper is as follows. First, in Sec. II, we give the details of the model construction, discuss the phase space partition, and characterize possible behavior of glued trajectories, including sliding motions. In Sec. III, we construct an explicit Poincaré return map that can be cast into a triangular form. In Secs. IV and V, we analyze the dynamics of this map and prove the existence of a singular hyperbolic strange attractor and explicitly point out major bifurcations associated with the emergence of the attractor. In Sec. VI, we close the loop by going back to the flow dynamics of our piecewise-smooth system and connect the dynamics of the Poincaré return map to the trajectories of the original ODE system. By doing so, we give analytical proofs of bifurcations leading to the birth of the strange attractor and explicitly link these bifurcations to the system's parameters. Section VII provides concluding remarks.

## II. PIECEWISE-SMOOTH MODEL AND ITS PROPERTIES

The application of our approach to constructing a piecewise-smooth ODE system that reproduces known, possibly chaotic dynamics of a given ODE requires particular skills and a certain kind of finesse for constructing homoclinic and saddle orbits. However, a general recipe can be given in the spirit of a school project which begins with a “shoe box,” “colored wires,” and “glue” (see Fig. 1 to appreciate the analogy). The recipe is as follows: (I) Identify fixed points of the given system and partition the phase space into the corresponding regions each containing one fixed point (cut the shoe box, add internal sections, and assign a color to each partition); (II) for each fixed point, write a normal form that describes linear dynamics around the fixed point and let this system govern all trajectories in the corresponding partition of the phase space (cut and install the wires (trajectories) according to their color coding); (III) arrange for switching from one linear system to another at the separating sections to ensure the continuity of one trajectory by another from the

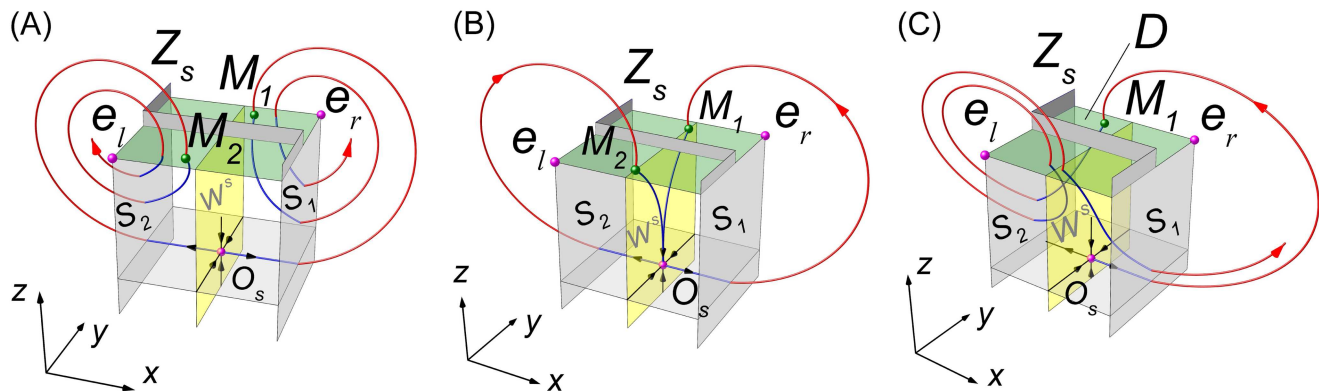


**FIG. 1.** The evolution of the unstable one-dimensional manifolds of saddle  $O_s$  as a function of parameters  $b$  and  $\nu$ . The phase space is partitioned into three regions  $G_s$ ,  $G_l$ , and  $G_r$  (not shown). The box-shaped saddle area is formed by the vertical half-planes  $S_1$  and  $S_2$  and the horizontal section  $D$  (green plane). The left and right focus regions are separated by the saddle region and the Z-shaped section  $Z_s$ . Stable foci  $e_l$  and  $e_r$  determine the dynamics in the focus regions. Emanating from  $O_s$ , the unstable manifold is composed from the parts of the saddle (blue) and focal (red) trajectories. (a)  $b = 1.6 < b_h$ ,  $\nu = 0.65$ . Point  $M_1$  lies in the region  $x > 0$ . The saddle part of the manifold  $W^u_1$  with the initial point  $M_1$  returns to the boundary  $S_1$  (blue part of the trajectory). (b)  $b = b_h = 2$ ,  $\nu = 0.65$ . Point  $M_1$  falls on the stable manifold  $W^s$  so that  $W^u_1$  returns to  $O_s$  and forms the right homoclinic orbit. Similarly, the left symmetrical unstable manifold  $W^u_2$  continued from point  $M_2$  forms the left homoclinic orbit, completing the homoclinic butterfly. (c)  $b = 2.6$ ,  $\nu = 0.9$ . Point  $M_1$  falls into the region  $x < 0$ . The saddle part of  $W^u_1$  originating from point  $M_1$  switches to the left and heads toward the left focus  $e_l$ . The trajectories are calculated numerically. Other parameters are  $\alpha = 2$ ,  $\lambda = 0.294$ ,  $\omega = 2$ , and  $\delta = 0.588$ .

different phase partition (connect and glue the colored wires at the separating sections); (IV) tweak the normal forms and adjust the partitions for a desired result. In more scientific terms, the construction of the piecewise-smooth system originates from the knowledge of the dynamics and bifurcations of the Poincaré return map which informs the phase space partition and the choice of specific linear systems.

In the following, we will start with the description of our switching piecewise-smooth ODE system and then construct a Poincaré return map which will be used for elucidating the main bifurcations and chaoticity of the attractor. However, in a historical retrospective, we first designed the simplest Poincaré return map which reproduced the main properties and bifurcations of the Lorenz system and then synthesized the ODE system, which matches the Poincaré return map, according to the recipe described above.

**A. Model construction**

We construct our switching piecewise-smooth system from the following three-dimensional linear subsystems  $A_s, A_l,$  and  $A_r$ :

$$\begin{aligned}
 A_s : \quad & \begin{cases} \dot{x} = x, \\ \dot{y} = -\alpha y, \\ \dot{z} = -\nu z, \end{cases} & (x, y, z) \in G_s, \\
 A_l : \quad & \begin{cases} \dot{x} = -\lambda(x + 1) + \omega(z - b), \\ \dot{y} = -\delta(y + 1), \\ \dot{z} = -\omega(x + 1) - \lambda(z - b), \end{cases} & (x, y, z) \in G_l, \\
 A_r : \quad & \begin{cases} \dot{x} = -\lambda(x - 1) - \omega(z - b), \\ \dot{y} = -\delta(y - 1), \\ \dot{z} = \omega(x - 1) - \lambda(z - b), \end{cases} & (x, y, z) \in G_r,
 \end{aligned} \tag{1}$$

where  $\alpha, \delta, \nu, \omega, \lambda,$  and  $b$  are positive parameters. These subsystems are defined in the following partitions of the system’s phase space,  $G_s, G_l,$  and  $G_r,$  respectively:

$$\begin{aligned}
 G_s : & |x| < 1, y \in \mathbb{R}^1, z < b, \\
 G_l : & \begin{cases} x \leq -1 & \text{for } z \leq b, \\ x \leq -1 & \text{for } z > b \text{ and } y \geq 0, \\ x < 1 & \text{for } z > b \text{ and } dy < 0, \end{cases} \\
 G_r : & \begin{cases} x \geq 1 & \text{for } z \leq b, \\ x \geq 1 & \text{for } z > b \text{ and } y < 0, \\ x > -1 & \text{for } z > b \text{ and } y \geq 0. \end{cases}
 \end{aligned} \tag{2}$$

As the original Lorenz system, system (1) is invariant under the involution  $(x, y, z) \rightarrow (-x, -y, z)$  and has three equilibria. The linear subsystem  $A_s$  governs the dynamics of system (1) in the region  $G_s$ . This system has a saddle fixed point  $O_s$  at the origin; therefore, we code-name  $G_s$  a saddle region. The subsystems  $A_{r,l}$  are defined in the regions  $G_{r,l}$  and have symmetrical equilibria  $e_{r,l} = \{\pm 1, \pm 1, b\}$ , respectively. These equilibria are stable three-dimensional foci in the subsystems  $A_{r,l}$  but may change their stability in full system (1). We code-name  $G_r$  and  $G_l$  as right and left focus regions, respectively.

The saddle region  $G_s$  is bounded on the right and left by the vertical half-planes  $S_1 = \{x = 1, y \in \mathbb{R}^1, z < b\}$  and  $S_2 = \{x = -1, y \in \mathbb{R}^1, z < b\}$  (see Fig. 1). It is also bounded from above by the part

of the plane  $D = \{|x| \leq 1, y \in \mathbb{R}^1, z = b\}$  (the green horizontal plane in Fig. 1). Below the plane  $D$ , the focus regions  $G_l$  and  $G_r$  are located to the left and right of the vertical half-planes  $S_2$  and  $S_1$ , respectively. Above the plane  $D$  where there is no saddle region, the focus regions are separated by the gray Z-shaped boundary  $Z_s$  (see Fig. 1).

Note that the linear subsystems  $A_s, A_l,$  and  $A_r$  composing system (1) are normal forms for a three-dimensional saddle and two stable foci, respectively, and have simple analytical solutions. Namely, the solution of the saddle system  $A_s$  with initial conditions in the plane  $D$  with  $z(0) = b$  is

$$\begin{aligned}
 x(t) &= x(0)e^t, \\
 y(t) &= y(0)e^{-\alpha t}, \\
 z(t) &= be^{-\nu t}.
 \end{aligned} \tag{3}$$

The solution of the focus system  $A_r$  with initial conditions  $x(0) = x_0 = 1, y(0) = y_0, z(0) = z_0$  on  $S_1$  has the form

$$\begin{aligned}
 x(t) &= 1 + (b - z_0)e^{-\lambda t} \sin(\omega t), \\
 y(t) &= 1 + (y_0 - 1)e^{-\delta t}, \\
 z(t) &= b - (b - z_0)e^{-\lambda t} \cos(\omega t).
 \end{aligned} \tag{4}$$

Similarly, the solution of the focus system  $A_l$  with initial conditions  $x(0) = -1, y(0) = y_0, z(0) = z_0$  on  $S_2$  is defined by

$$\begin{aligned}
 x(t) &= -1 - (b - z_0)e^{-\lambda t} \sin(\omega t), \\
 y(t) &= -1 + (y_0 + 1)e^{-\delta t}, \\
 z(t) &= b - (b - z_0)e^{-\lambda t} \cos(\omega t).
 \end{aligned} \tag{5}$$

The equilibria  $e_{r,l}$  lie on the boundaries of the  $G_{r,l}$  and  $G_s$  regions where the intersections of the regions are the invariant lines  $l_r = (x = 1, z = b)$  and  $l_l = (x = -1, z = b)$ . Trajectories in vicinities of the equilibria are composed (glued) from the trajectories of the focus systems  $A_{r,l}$  and saddle system  $A_s$  defined through (3), (4), and (5). Depending on the system’s parameters, the balance between the saddle and focal parts of the trajectories can change. Increasing parameter  $b$  transforms stable foci  $e_{r,l}$  into saddle foci, as will be shown later in the paper. In light of this, it is worth emphasizing the importance of placing the equilibria  $e_{r,l}$  on boundaries of  $G_{r,l}$  and  $G_s$ , thereby allowing the equilibrium  $e_{r,l}$  to change their stability. Shifting these equilibria from the boundaries so that the vicinity of  $e_{r,l}$  entirely belongs to the focal parts of the phase space would make  $e_{r,l}$  stable foci for any positive values of  $\alpha, \delta, \nu, \omega, \lambda, b,$  and, therefore, would prevent the piecewise-smooth system (1) from having a Lorenz-type chaotic attractor. The possibility remains that a complex attractor, which contains stable sliding motions on the boundaries  $G_r$  and  $G_l$ , may appear and coexist with the stable foci.

The saddle  $O_s$  has a two-dimensional stable manifold defined in the saddle region by  $W_{saddle}^s = \{x = 0, y \in \mathbb{R}^1, z < b\}$  (the yellow vertical plane in Fig. 1) and a one-dimensional unstable manifold, defined in the saddle region by  $W_{1saddle}^u = \{0 < x < 1, y = z = 0\}$  and  $W_{2saddle}^u = \{-1 < x < 0, y = z = 0\}$ . These manifolds and their continuations along the trajectories of systems  $A_{r,l}$  in the focus regions form the global manifolds  $W^s, W_1^u,$  and  $W_2^u$  of the saddle  $O_s$  in the full phase space of system (1).

By construction, the section  $D$  with  $z = b$  is equivalent to the global cross-section  $z = \rho - 1$  in the original Lorenz system<sup>15</sup>

$$\dot{x} = \sigma(y - x), \quad \dot{y} = \rho x - y - xz, \quad \dot{z} = xy - \beta z. \quad (6)$$

Therefore, the parameter  $b$  in the piecewise-smooth system (1) plays a role of  $\rho - 1$  in the Lorenz system (6). Notice that the eigenvalues of the saddle  $O_L(0, 0, 0)$  in the Lorenz system are  $m_{1,2} = -\frac{1}{2}[\sigma + 1 \pm \sqrt{(\sigma - 1)^2 + 4\sigma\rho}]$ , where the positive (negative) sign corresponds to  $m_1$  ( $m_2$ ), and  $m_3 = -\beta$ . Therefore, diagonalizing the linearized system in the vicinity of the saddle  $O_L$  yields

$$\dot{u} = u, \quad \dot{w} = \frac{m_2}{m_1} w, \quad \dot{z} = -\frac{\beta}{m_1} z, \quad (7)$$

where  $u$  and  $w$  are new variables corresponding to the eigenvectors associated with eigenvalues  $m_1$  and  $m_2$ , respectively, and  $z$  is the original variable corresponding to  $m_3$  since the  $z$  axis is an invariant line of (6). In (7), the time derivative is calculated with respect to the new time  $\hat{t} = t/m_1$ . Comparing the linearized system (7) for the saddle  $O_L$  in the Lorenz system with the normal form  $A_s$  for the saddle  $O_s$  in the piecewise-smooth system (1) suggests that the parameters  $\alpha$  and  $\nu$  in (1) are equivalent to  $-m_2/m_1$  and  $\beta/m_1$  in the Lorenz system (6), respectively. The other parameters  $\lambda, \omega, \delta$  of system (1) control the focus systems  $A_l$  and  $A_r$  and do not have direct analogs in the Lorenz system (6).

Throughout the paper, we assume that the parameters satisfy the conditions

$$\frac{1}{2} < \nu < 1 < \alpha. \quad (8)$$

The part of this inequality  $\nu < 1$  implies that the saddle value of the saddle  $O_s$ ,  $\eta = 1 - \nu > 0$ . The additional inequality  $1 < \alpha$  pushes the eigenvalues 1 and  $-\nu$  to be nearest to zero and, therefore, makes the plane  $W^{lead} = ((x, z) \in G_s, y = 0)$  determine the leading (weaker) direction as a piece of the leading stable manifold  $W^s$ . This property is chosen to match the property of the original Lorenz system, which allows  $W_1^u$  and  $W_2^u$  to form desired homoclinic orbits and lead to the emergence of complex dynamics.<sup>59</sup> The origin of the remaining part of the inequality  $1/2 < \nu$  will be explained in Sec. IV (see Remark 2).

### B. Gluing the trajectories

Trajectories of the piecewise-smooth system (1) are composed of trajectories of systems  $A_s$ ,  $A_r$ , and  $A_l$ , which are explicitly given by the solutions (3), (4), and (5). We demonstrate the gluing process through constructing the one-dimensional unstable manifold  $W_1^u$  emanating from the saddle  $O_s$  in the region  $G_s$ , extending to the region  $G_r$ , and eventually spiraling out in  $G_l$  and  $G_r$  [see Fig. 1(a)].

We start from the saddle  $O_s$  and follow the unstable manifold  $W_1^u$  in the direction of the vertical half-plane  $S_1$ . The part of the manifold in the saddle region is defined through (3) (a blue line segment in Fig. 1). The manifold intersects the half-plane  $S_1$  at the point  $(x_0 = 1, y_0 = 0, z_0 = 0) \in S_1$ , which becomes its exit point from the region  $G_s$ . This point becomes the initial condition for the solution (4), which continues the manifold  $W_{saddle}^u$  as it enters into the right focus region  $G_r$  (the red curve ending at the point  $M_1$  in Fig. 1). When the focal part of the unstable manifold reaches the point  $M_1$  that lies on the upper boundary of the saddle region  $G_s$ , the plane  $D$  (the green

plane in Fig. 1), the trajectory is further continued by a trajectory defined through the saddle system  $A_s$  (the right blue curved line in Fig. 1). The shape of the glued unstable manifold essentially depends on the location of the point  $M_1$  with respect to the stable manifold of the saddle  $W^s$  (the yellow vertical plane in Fig. 1) [compare the trajectories in Figs. 1(a) and 1(c)].

As it will be rigorously shown in Sec. VI, the relative location of point  $M_1$  with respect to  $W^s$  is controlled by the parameter  $b$ , which is hereafter chosen as a bifurcation parameter. For small  $b$ , the point  $M_1$  lies in the region  $x > 0$  and the saddle trajectory originating from the point  $M_1$  returns the unstable manifold  $W_1^u$  to the region  $G_r$  [see Fig. 1(a)]. Note that increasing the parameter  $b$  in the system  $A_r$  makes the focal part of the glued unstable manifold larger. As a result, for some  $b = b_h$ , the point  $M_1$  falls on the stable manifold  $W^s$ , and the unstable manifold  $W_1^u$  becomes a homoclinic orbit of saddle  $O_s$  [see Fig. 1(b)]. This value  $b_h$  will be explicitly derived in terms of the other system's parameters in Sec. VI.

With further increase in  $b > b_h$ , the point  $M_1$  crosses the border line and falls into the region  $x < 0$ . In this case, the saddle trajectory [the blue line in Fig. 1(c)] originating from point  $M_1$  brings the unstable manifold  $W_1^u$  to the left focus region  $G_l$ . Sequential continuation of this unstable manifold along the focal trajectory of the left focus system  $A_l$  [the red line in Fig. 1(c)] takes it to the  $y < 0$  part of the plane  $D$ . Further continuation of the one-dimensional manifold  $W_1^u$  to the saddle region  $G_s$  either brings it to the region  $G_l$ , or immediately returns the manifold to the region  $G_r$  [see Fig. 1(c)]. By virtue of the system's symmetry, the shape of the unstable saddle manifold  $W_2^u$  mirrors that of  $W_1^u$  [not shown].

The homoclinic bifurcation of the symmetrical orbits of the saddle  $O_s$  at  $b = b_h$  leads to the birth of two saddle limit cycles  $C_1$  and  $C_2$  for  $b > b_h$  as in the original Lorenz system (the detailed bifurcation analysis is given in Sec. VI). These saddle limit cycles  $C_1$  and  $C_2$  are composed of two glued pieces where one piece is defined by a saddle trajectory (thick red curves in Fig. 2), whereas the other is determined by a stable focus trajectory (thick blue curves in Fig. 2). The prevalence of the saddle part of the trajectory over its focal part determines the overall saddle type of the limit cycles.

Other trajectories of system (1) not shown in Figs. 1 and 2 are constructed through the same gluing process at the boundaries of regions  $G_s$ ,  $G_r$ , and  $G_l$ , with the exception of trajectories that fall on the Z-shaped boundary  $Z_s$  and produce sliding motions. Figure 3 demonstrates a typical Lorenz-type attractor that appears in the piecewise-smooth system (1) as a result of this gluing process and switching among three linear systems  $A_s$ ,  $A_r$ , and  $A_l$  (a detailed description of the attractor's birth and properties is given in Sec. VI).

In the following, we will estimate the size of the system's absorbing domain which contains all of the system's attractors. We will characterize possible sliding motions and their location with respect to the absorbing domain. The reader willing to accept the claims that the sliding motions do not participate in the formation of the strange Lorenz-type attractor without proofs can proceed to Sec. III without loss of continuity.

### C. Absorbing domain

The following assertion proves eventual dissipativeness of system (1) and places an upper bound on the absorbing domain which traps all trajectories of system (1).

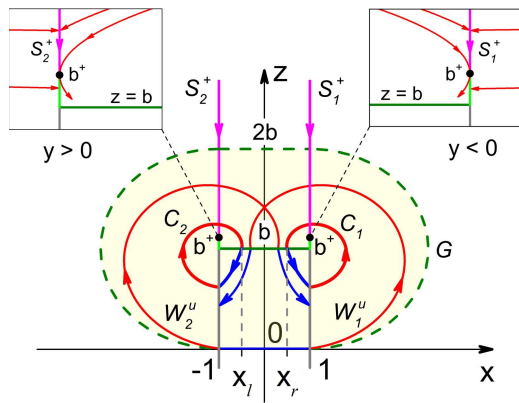


**FIG. 2.** The  $xz$  projection of the phase space similar to Fig. 1(c) at  $y = 0$ . The shaded area bounded by the dashed green curve is the absorbing domain  $G$ , plotted via (9). Two gray vertical lines at  $x = -1$  and  $x = 1$  correspond to the lateral boundaries  $S_1$  and  $S_2$  of the saddle region. The green horizontal line at  $z = b$  is the upper boundary  $D$  [cf. Fig. 1(c)]. Two saddle cycles  $C_1$  and  $C_2$  are formed by the parts of the saddle (blue) and focus (red) trajectories and born as a result of the homoclinic bifurcation. Two vertical pink lines are projections of the vertical half-planes  $S_1^+$  and  $S_2^+$  and correspond to stable sliding motions. Note that the trajectories (red lines) do not cross the stable sliding half-planes  $S_1^+$  and  $S_2^+$  such that the saddle cycle  $C_2$  appears in front of the projection of  $S_2^+$ , whereas  $C_1$  is behind the projection of  $S_1^+$ . (Inserts): Zoomed-in neighborhoods of points  $b^+$  and the local vector fields. The part of the sliding vertical segment between the point  $b^+$  and the global cross section (light green vertical line segment) is one-way passable for trajectories. All trajectories are calculated numerically. The parameters are  $b = 2.6$ ,  $\nu = 0.7$ ,  $\alpha = 2$ ,  $\lambda = 0.294$ ,  $\omega = 2$ , and  $\delta = 0.588$ .

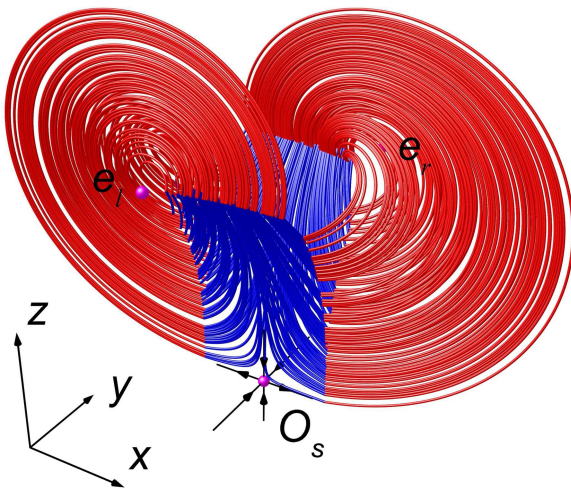


**FIG. 3.** A Lorenz-type attractor in the piecewise-smooth system (1). Chaotic trajectories are glued from pieces of saddle (blue) and focal (red) trajectories of three linear systems. Parameters  $b = 3.8$ ,  $\alpha = 2$ ,  $\nu = 0.75$ ,  $\lambda = 0.294$ ,  $\omega = 2$ , and  $\delta = 0.588$ .

**Lemma 1:** *The region*

$$G = \begin{cases} |y| \leq 1, \\ 0 \leq z \leq 2b & \text{for } |x| \leq 1, \\ V_l \leq b^2 & \text{for } x < -1, \\ V_r \leq b^2 & \text{for } x > 1, \end{cases} \quad (9)$$

with  $V_{l,r} = (x \pm 1)^2 + (z - b)^2$  is an absorbing domain which attracts all trajectories of system (1).

*Proof.* Our goal is to construct a Lyapunov-like function and identify its level at which the time derivative of the Lyapunov function along the trajectories of system (1) equals zero, thereby determining the boundary of the absorbing domain. As system (1) is piecewise-smooth, we assemble such a Lyapunov function from several functions that describe the behavior of the system in different partitions of the phase space.

Consider a Lyapunov function  $V_1 = y^2 - 1$  in the region  $|y| > 1$  where  $V_1$  is positive. Its time derivative with respect to system (1) is (i)  $\dot{V}_1 = -2\delta(y \pm 1) < 0$  for  $|y| > 1$ ,  $|x| > 1$ ; hereafter, the plus (minus) sign relates to the dynamics governed by the focus system  $A_l$  ( $A_r$ ) and (ii)  $\dot{V}_1 = -2\alpha y^2 < 0$  for  $|y| > 1$ ,  $|x| \leq 1$  which governs the trajectories of the saddle system  $A_s$ . Therefore, all trajectories enter the region  $|y| \leq 1$ .

Similarly, we choose a directing Lyapunov function  $V_2 = (z - b)^2 - b$  which is positive outside the interval  $0 < z < 2b$ . Recall that the trajectories of system (1) are governed by the focus systems  $A_l$  and  $A_r$  for  $z > b$ , and by all three saddle and focus systems  $A_s$ ,  $A_l$ , and  $A_r$  for  $z < b$ . Hence, outside the interval  $0 < z < 2b$  the time derivative of  $V_2$  with respect to (i) systems  $A_l$  and  $A_r$  is  $\dot{V}_2 = -2\lambda(z - b)^2 - 2\omega(z - b)(1 \pm x) < 0$  for  $|x| < 1$  and (ii) the saddle system  $A_s$  are  $\dot{V}_2 = -2\nu(z - b)z < 0$  in the region  $z < 0$ . Therefore, all trajectories enter the region  $0 < z < 2b$  for  $|x| \leq 1$ .

Finally, we choose a directing Lyapunov function  $V_3 = V_{l,r} - b^2$  which is positive in the intervals in question  $x < -1$  and  $x > 1$ , respectively. Its time derivative along the trajectories of the focus system  $A_l$ :  $\dot{V}_3 = -2\lambda V_1 < 0$  for  $x < -1$  and with respect to the focus system  $A_r$ :  $\dot{V}_3 = -2\lambda V_r < 0$  for  $x > 1$ . Hence, the trajectories from these regions cross the surfaces  $V_1$  and  $V_2$ .

Combining the bounds on the directing Lyapunov functions  $V_1$ ,  $V_2$ , and  $V_3$ , we obtain the absorbing domain  $G$ .  $\square$

### D. Sliding motions

Due to its piecewise-smooth nature, system (1) can have stable sliding motions. Toward our goal of constructing a Lorenz-type chaotic attractor which contains only saddle orbits, we seek to identify the system's parameters for which the stable sliding motions do not participate in the formation of the attractor.

The orientation of the vector fields of systems  $A_s$ ,  $A_r$ , and  $A_l$ , suggests the following.

1. The only (locally) stable sliding regions on the  $Z$ -shaped boundary  $Z_s$  are its parts  $S_1^+ = \{x = 1, z > b^+ = b + \frac{2\lambda}{\omega}, y < 0\}$  and  $S_2^+ = \{x = -1, z > b^+ = b + \frac{2\lambda}{\omega}, y > 0\}$  (the pink vertical lines in Fig. 2). This claim can be verified by checking the  $x$  directions of the vector flows of systems  $A_r$  and  $A_l$  at  $S_1^+$  and

$S_2^+$ . For example, consider the left half-plane  $S_2^+$  with  $x = -1$ . The local vector field to the right from this vertical half-plane  $S_2^+$  is governed by the focus system  $A_r$ . Therefore, this flow in the  $x$  direction is determined by  $\dot{x} = -\lambda(x - 1) - \omega(z - b)$  such that  $\dot{x} = 2\lambda - \omega(z - b)$  at  $S_2^+$  with  $x = -1$ . As a result,  $\dot{x} < 0$  at  $S_2^+$  for the right focus system  $A_r$  and the corresponding vector flow is oriented toward  $S_2^+$  as long as  $z > b^+ = b + \frac{2\lambda}{\omega}$ . Then, for  $z < b^+$ , the flow to the right from  $S_2^+$  reverses its  $x$  direction and points to the right (see the left zoom-in in Fig. 2). At the same time, the vector field to the left from  $S_2^+$  and its extension down to the section  $D$  at  $z = b$  is oriented in the positive  $x$  direction and preserved in the interval  $b < z < b^+$ . This is due to the fact that this vector field is governed by the focus system  $A_l$  so that its  $x$  direction at  $S_2^+$  with  $x = -1$  is defined through  $\dot{x} = \omega(z - b)$ , which is positive on the boundary  $Z_s$  at  $x = -1$  everywhere above the section  $D$  (for  $z > b$ ). As a result, the half-plane  $S_2^+$  locally attracts trajectories from its left and right and yields locally stable sliding motions. The extension of  $S_2^+$  from  $z = b^+$  down to  $D$  (the bright green segment in the left zoom-in of Fig. 2) is passable for the trajectories approaching it from the left as the vector fields from the left and right point in the same direction of positive  $x$ .

Similarly, due to the system's symmetry, the half-plane  $S_1^+$  corresponds to locally stable sliding motions, and its extension to  $D$  is passable (see the right zoom-in in Fig. 2).

- The middle section of the  $Z$ -shaped boundary ( $y = 0, |x| < 1, z \geq b$ ) only contains unstable sliding motions. This can be verified by checking the  $y$  equations of the focus systems  $A_l$  and  $A_r$  at  $y = 0$ . The negative and positive signs of  $\dot{y}$  in  $A_l$  and  $A_r$ , respectively, indicate that the local vector fields of both systems point out from the middle section of  $Z_s$ , making it unstable.

To determine the eventual behavior of sliding trajectories on the stable half-planes  $S_{1,2}^+$ , we follow Filippov's approach<sup>60</sup> and define sliding motion on  $S_{1,2}^+$  through a  $(y, z)$  system obtained by averaging the corresponding  $\dot{y}$  and  $\dot{z}$  components of the  $A_l$  and  $A_r$  systems. These average systems calculated for  $S_2^+$  with  $x = -1$  and  $S_1^+$  with  $x = 1$  happen to be the same and take the form

$$\begin{aligned} \dot{y} &= (\dot{y}_l + \dot{y}_r)/2 = -\delta y, \\ \dot{z} &= (\dot{z}_l + \dot{z}_r)/2 = -\omega - \lambda(z - b), \end{aligned} \tag{10}$$

where  $y_l$  and  $z_r$  ( $y_r$  and  $z_r$ ) correspond to the variables of the  $A_l$  ( $A_r$ ) system.

The linear system (10) has a unique globally stable equilibrium  $E = (y = 0, z = b - \frac{\omega}{\lambda})$  that is located below the point  $b^+$  where the stable sliding half-planes  $S_{1,2}^+$  terminate. Hence, this globally stable point  $E$  enables the downward sliding motion everywhere on  $S_{1,2}^+$ . Thus, when all trajectories slide down along  $S_{1,2}^+$  and reach  $b^+$ , they continue to be pushed down toward  $E$ . Once the trajectories enter the downward extension of  $S_{1,2}^+$  which is passable, they leave the sliding motion half-planes and eventually reach the cross-section  $D$  (see the zoom-ins in Fig. 2).

Toward our goal of proving the emergence of a strange chaotic attractor without stable trajectories, we need to identify a set of the

system's parameters where the stable sliding motions on the half-planes  $S_{1,2}^+$  do not belong to the attractor. This leads to the following statement.

**Theorem 1:** *Attractors of system (1) contain no sliding motions in the parameter region*

$$\begin{aligned} \delta &> \delta_{cr} = \frac{\omega \ln 2}{\pi}, \\ b &< b_{cr} = 2\sqrt{1 + \frac{\lambda^2}{\omega^2}} \exp\left\{\frac{\lambda}{\omega}\left(\arctan \frac{\omega}{\lambda} + \pi\right)\right\}. \end{aligned} \tag{11}$$

*Proof.* In order for any attractor of system (1) not to contain sliding motions, we require that any trajectory with initial conditions on the global cross-section  $D$  never falls on the  $Z$ -shaped boundary  $Z_s$  (cf. Fig. 1), which glues the regions  $G_l$  and  $G_r$  and is the origin of sliding motions.

The points on the cross-section  $D$  are transferred by trajectories of the saddle region  $G_s$  to its lateral boundaries  $S_1$  and  $S_2$  so that the trajectories may not reach  $Z_s$ . Therefore, the problem of bypassing the boundary  $Z_s$  is reduced to finding a parameter region of the focus systems  $A_l$  and  $A_r$  where the trajectories starting from  $S_1$  and  $S_2$  return to  $D$ , avoiding  $Z_s$ .

As it was demonstrated above, the middle section of  $Z_s$  is unstable and, therefore, unreachable so that we should only worry about trajectories that may reach the stable sliding half-planes  $S_{1,2}^+$  which are contained in  $Z_s$ . Due to Lemma 1, the system's absorbing domain  $G$  does not expand beyond the interval  $|y| \leq 1$  in the  $y$  direction and is limited by  $z = 2b$  in the  $z$  direction at  $x = \pm 1$ . Hence, only parts of the half-planes  $S_{1,2}^+$  that belong to the absorbing domain matter. These parts are

$$\begin{aligned} S_{1a}^+ &: \{x = 1, -1 < y < 0, b^+ < z < 2b\}, \\ S_{2a}^+ &: \{x = -1, 0 < y < 1, b^+ < z < 2b\}. \end{aligned} \tag{12}$$

For definiteness, consider trajectories that initiate from the part of the half-plane  $S_1$  that belongs to the absorbing domain  $S_{1a}$ :  $\{x = 1, -1 < y < 0, z < b\}$ . These trajectories are continued by the focus system  $A_r$ . To avoid the presence of the sliding motions inside the attractor, all trajectories leaving  $S_{1a}$  should (i) not land on the right vertical segment  $S_{1a}^+$  and (ii) not reach the left vertical segment  $S_{2a}^+$ . We shall derive bounds on the system's parameters for each of the two cases separately.

**Bound 1.** Each trajectory with initial conditions on the vertical segment  $S_{1a}$  with  $x = 1$  will either return to  $S_{1a}$  or reach the extension of  $S_{1a}$  with  $x = 1$  in the region  $z > b$  in time  $\tau_1 = \pi/\omega$ . This extension is comprised of two parts: the stable sliding motion segment  $S_{1a}^+$  for  $-1 < y < 0$  and the nonsliding part for  $y > 0$ . The time constant  $\tau_1 = \pi/\omega$  comes from solving the  $x$  equation of system (4) with the initial  $(x(0) = 1)$  and final  $(x(\tau_1) = 1)$  states, as the trajectory departs from and comes back to the plane  $x = 1$ . We seek to find the conditions under which each trajectory leaving  $S_{1a}$  reaches the plane  $x = 1$  at  $y(\tau_1) > 0$  and, therefore, lands on its nonsliding part. It is important to emphasize that if a trajectory with the initial condition  $y(0) = -1$  on the absorbing domain's border  $y = 1$  is transferred by the focus linear system  $A_r$  far enough to enter the region  $y > 0$  with no sliding motions, then all other trajectories starting from  $S_{1a}$  with  $-1 < y < 0$  will go even farther and will also miss the sliding region



$S_{1a}^+$ . Solving the  $y$  equation of system (4) with the initial condition  $y(0) = -1$  yields the solution  $y(t) = 1 - 2e^{-\delta t}$ . Substituting the time constant  $\tau_1 = \pi/\omega$  and requiring  $y(\pi/\omega) > 0$ , we arrive at the condition  $\delta > \delta_{cr} = \frac{\omega \ln 2}{\pi}$ , which guarantees that each trajectory starting from  $S_{1a}$  will not land on the sliding motion segment  $S_{1a}^+$ .

**Bound 2.** We seek to identify a set of parameters which guarantee that trajectories launching from  $S_{1a}$  cannot reach the left vertical half-plane  $S_2^+$  that corresponds to stable sliding motions. These trajectories of the focus system  $A_r$  with initial points at  $S_{1a}$  are bounded in  $(x, z)$  by a two-dimensional surface composed of trajectories with initial conditions  $x = 1, |y| \leq 1$ , and  $z = 0$ . In particular, the unstable manifold  $W_1^u$  of saddle  $O_s$  belongs to this surface. Therefore, it is sufficient to demonstrate that if the unstable manifold  $W_1^u$  does not extend to  $S_2^+$ , then any other trajectory starting from  $S_{1a}$  cannot reach  $S_2^+$  either. The unstable manifold  $W_1^u$  emanating from  $O_s$  intersects  $S_{1a}$  at the point  $x = 1, y = 0, z = 0$  and then is continued by the focus system  $A_r$ . Therefore, the corresponding  $x$  and  $z$  solutions (4) of the focus system  $A_r$  with the initial  $(x(0) = 1, z(0) = 0)$  and final  $(x(\tau_2) = -1, z(\tau_2) = b^+ = b + \frac{2\lambda}{\omega})$  states yield the conditions

$$\begin{aligned} e^{-\lambda\tau_2} \sin(\omega\tau_2) &= -\frac{2}{b_{cr}}, \\ e^{-\lambda\tau_2} \cos(\omega\tau_2) &= -\frac{2\lambda}{\omega b_{cr}}, \end{aligned} \tag{13}$$

which define the critical value  $b_{cr}$  of parameter  $b$  for which  $W_1^u$  can still be tangent to the end point  $b^+ = b + \frac{2\lambda}{\omega}$  of the half-plane  $S_2^+$  (see the left zoom-in in Fig. 2). Dividing the first equation by the second equation in (13) yields the time  $\tau_2 = \frac{1}{\omega} \arctan \frac{\omega}{\lambda}$ . Substituting  $\tau_2$  into (13) and using the trigonometric identity, we obtain

$$b_{cr} = 2\sqrt{1 + \frac{\lambda^2}{\omega^2}} \exp \left\{ \frac{\lambda}{\omega} \left( \arctan \frac{\omega}{\lambda} + \pi \right) \right\}. \tag{14}$$

Thus, for  $b < b_{cr}$ , the unstable manifold  $W_1^u$  and all other trajectories starting from  $S_{1a}$  have no tangency with the stable sliding half-plane  $S_2^+$  and hit the cross-section  $D$  without reaching  $S_2^+$ . Due to the system's symmetry, the same argument carries over to the trajectories starting from  $S_2$  which are governed by the focus system  $A_l$ .  $\square$

### III. POINCARÉ RETURN MAP: THE CONSTRUCTION

Following the steps of the classical studies of the Lorenz system,<sup>6-13</sup> we will construct a flow-defined Poincaré return map that allows for characterizing a bifurcation sequence that leads to the birth of the Lorenz-type attractor and prove the chaoticity of the attractor. This Poincaré return map possesses a unique property of being explicitly given by glued, closed-form solutions of the piecewise-smooth system (1). To construct the Poincaré map, we choose  $D = \{|x| \leq 1, |y| \leq 1, z = b\}$  as a Poincaré cross section and analyze how this section is mapped into itself by trajectories of the saddle and focus systems. We choose the parameters that satisfy the condition of Theorem 1, which guarantees that trajectories of systems  $A_r$  and  $A_l$  starting from  $S_{1,2}$  may not reach the stable sliding regions  $S_{1,2}^+$ . Therefore, under the conditions (11),  $D$  is a global cross section such that all

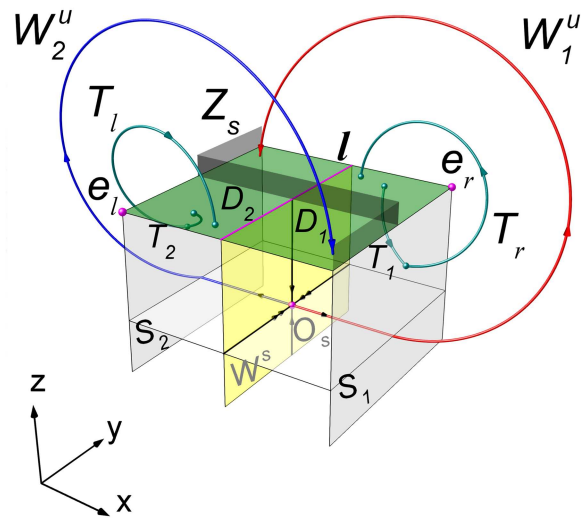


**FIG. 4.** The construction of the Poincaré return map (20). The cross-section  $D = D_1 \cup D_2$  (green) is mapped into itself by trajectories of the piecewise-smooth system (1). The initial point (green dot) in  $D_1$  ( $D_2$ ) is first mapped into the vertical half-plane  $S_1$  ( $S_2$ ) by the map  $T_1$  ( $T_2$ ). Its image in  $S_1$  ( $S_2$ ) is then mapped into the cross-section  $D$  by the map  $T_r$  ( $T_l$ ). The line  $l = W^s \cap D : x = 0$  (pink) is a singularity line whose image is two points of intersection between  $D = D_1 \cup D_2$  and unstable manifolds  $W_1^u$  (red) and  $W_2^u$  (blue). The meaning of blue and red color coding (left vs right trajectories) differs from that of Figs. 1-3 (saddle vs focal parts).

trajectories starting from  $D$  will return back to it. The cross-section  $D$  is divided into two symmetrical parts,  $D_1 = D|_{x \geq 0}$  and  $D_2 = D|_{x \leq 0}$ , by the stable manifold  $W^s$  of the saddle  $O_s$  along the line  $l = W^s \cap D$  (see Fig. 4).

We shall first derive the Poincaré return map  $F_1 = T_r T_1$  of the half-section  $D_1$  as a composition of the maps  $T_1 : D_1 \rightarrow S_1$  and  $T_r : S_1 \rightarrow D$ . Here, the map  $T_1$  is generated by the trajectories of the saddle system that transfer points from the half-section  $D_1$  to the vertical half-plane  $S_1$ . Their subsequent transfer from  $S_1$  back to  $D$  by the trajectories of the focus system  $A_r$  yields the map  $T_r$ . Once we establish an explicit form of  $F_1 = T_r T_1$ , we will be able to obtain its complement map  $F_2 = T_l T_2, D_2 \rightarrow D$ , which is odd symmetrical to  $F_1$ . Thus, we shall first concentrate on the derivation of  $F_1$ .

Using the solution (3) of system  $A_s$  with the initial conditions in  $D_1$  such that  $z(0) = 0$  and the final boundary conditions  $(x(\tau) = 1, y(\tau), z(\tau)) \in S_1$ , we obtain the transition time  $\tau$  and coordinates in  $S_1$  as follows:

$$\begin{aligned} \tau &= -\ln x(0), \\ y(\tau) &= y(0)e^{-\alpha\tau}, \\ z(\tau) &= be^{-\nu\tau}. \end{aligned} \tag{15}$$

Substituting  $\tau$  into the  $y$  and  $z$  equations, we derive the explicit form of the map  $T_1$

$$\begin{aligned} T_1 : \quad y(\tau) &= y(0)e^{\alpha \ln x(0)} = y(0)x^\alpha(0), \\ z(\tau) &= be^{\nu \ln x(0)} = bx^\nu(0). \end{aligned} \tag{16}$$

To construct the map  $T_r : S_1 \rightarrow D$ , we analyze the solution (4) of the system  $A_r$  with the initial  $(\{x = 1, z = z_0, y = y_0\} \in S_1)$  and the final boundary  $(\{x(\tau'), y(\tau'), z(\tau')\} \in D)$  conditions where  $\tau' = \frac{3\pi}{2\omega}$  is the travel time from  $S_1$  to  $D$ . Note that the value of  $\tau'$  originates from the condition  $\cos \omega \tau' = 0$  obtained by setting  $z(\tau') = b$  in the  $z$ -equation of (4) where  $\tau' = \frac{3\pi}{2\omega}$  corresponds to the desired intersection of the plane  $z = b$  from above. Thus, we obtain the map  $T_r$

$$T_r : \begin{cases} x(\tau') = 1 - (b - z_0)e^{-\frac{3\pi\lambda}{2\omega}}, \\ y(\tau') = 1 + (y_0 - 1)e^{-\frac{3\pi\delta}{2\omega}}. \end{cases} \quad (17)$$

To close the loop in deriving the composition map  $F_1 = T_r T_1 : D_1 \rightarrow D$ , we replace  $y_0$  and  $z_0$  in (17) with  $y(\tau)$  and  $z(\tau)$  from (16), respectively, and obtain the explicit form of the map  $F_1$

$$F_1 : \begin{cases} \bar{x} = 1 + be^{-\frac{3\pi\lambda}{2\omega}}(x^v - 1), \\ \bar{y} = 1 + e^{-\frac{3\pi\delta}{2\omega}}(x^\alpha y - 1), \end{cases} \quad (18)$$

where  $x = x(0), \bar{x} = x(\tau'), y = y(0)$ , and  $\bar{y} = y(\tau')$ .

Due to the odd symmetry in  $x$  and  $y$ , the explicit form of the map  $F_2 : D_2 \rightarrow D$  can be obtained from (18) by replacing  $(x, y)$  with  $(-x, -y)$ . For convenience, we introduce two new parameters

$$\gamma = be^{-\frac{3\pi\lambda}{2\omega}}, \quad r = e^{-\frac{3\pi\delta}{2\omega}} \quad (19)$$

such that the complete map  $F : D \rightarrow D$  takes the form

$$F : \begin{cases} \bar{x} = f(x) \equiv 1 - \gamma + \gamma x^v, \\ \bar{y} = g(x, y) \equiv 1 - r + rx^\alpha y, & \text{for } x > 0, \\ \bar{x} = f(x) \equiv \gamma - 1 - \gamma |x|^v, \\ \bar{y} = g(x, y) \equiv r - 1 + r|x|^\alpha y, & \text{for } x < 0. \end{cases} \quad (20)$$

The map  $F$  is discontinuous at  $x = 0$  so that the line  $l = W^s \cap D : x = 0$  is mapped into the saddle point  $O_s$  and, therefore, points on  $l$  do not return back to the cross-section  $D$ . However, points from an infinitesimal neighborhood of line  $l$ ,  $(x = \pm \varepsilon, y \in [-1, +1])$  do return to  $D$ , passing by a close vicinity of the saddle point  $O_s$ . In the limit of  $\varepsilon \rightarrow 0$ , the images of these points are two points  $M_1$  and  $M_2$  (Fig. 1), which are the intersections of the cross-section  $D$  with the one-dimensional unstable manifolds  $W_1^u$  for  $x > 0$  and  $W_2^u$  for  $x < 0$ , respectively. By continuity, we define the map  $F$  at the discontinuity line  $l : (x = 0, y \in [-1, +1])$  as follows:

$$F|_{x=0} : \begin{cases} (\bar{x}, \bar{y}) = M_1(1 - \gamma, 1 - r) & \text{for } x \rightarrow +0, \\ (\bar{x}, \bar{y}) = M_2(\gamma - 1, r - 1) & \text{for } x \rightarrow -0. \end{cases} \quad (21)$$

Note that for  $\gamma = 1$  ( $b = b_h = e^{\frac{3\pi\lambda}{2\omega}}$ ) the unstable manifolds  $W_1^u$  and  $W_2^u$  place the points  $M_1$  and  $M_2$  on the line  $x = 0$  and, therefore, form two homoclinic orbits of the saddle  $O_s$  [see Fig. 1(b)]. Finally, to make the map  $F$  well-defined, hereafter we assume that the parameters  $r$

and  $\gamma$  satisfy the conditions

$$\begin{aligned} r &< \frac{1}{2\sqrt{2}}, \\ \gamma &< \gamma_{cr} = 2\sqrt{1 + \frac{\lambda^2}{\omega^2}} \exp\left\{\frac{\lambda}{\omega}\left(\arctan \frac{\omega}{\lambda} - \frac{\pi}{2}\right)\right\}. \end{aligned} \quad (22)$$

These conditions correspond to the parameter range (11) that guarantees the absence of sliding motions in any attractor of the flow system (1) and hence of the map  $F$ .

Observe that the map  $F$  has a triangular form such that the  $x$  equation of the map  $F, \bar{x} = f(x)$ , does not depend on  $y$  and drives its  $y$  equation. Therefore, we call the 1-D map  $\bar{x} = f(x)$  the “master” map. The triangular form of the 2D map  $F$  which naturally yields the 1-D master map is a key property which significantly simplifies our rigorous analysis. The appearance of this triangular form is rooted in the use of the normal forms which uncouple the  $x$  and  $z$  variables from the  $y$  variable in the focus systems  $A_{l,r}$  in (1). As a result, the corresponding dynamics along the  $x$  and  $z$  directions are independent from the motion along the  $y$  axis.

In the following, we will first study attractors and bifurcation properties of this master map to eventually reveal the properties of the complete 2D map  $F$  and ultimately prove the emergence of a chaotic Lorenz-type attractor in the original flow system (1).

#### IV. DYNAMICS OF THE 1-D MASTER MAP

Obtained from (20), the 1-D master map has the form

$$\begin{aligned} \bar{x} = f(x) &\equiv 1 - \gamma + \gamma x^v & \text{for } x > 0, \\ \bar{x} = f(x) &\equiv \gamma - 1 - \gamma |x|^v & \text{for } x < 0, \end{aligned} \quad (23)$$

where  $\bar{x}$  indicates the subsequent iterate  $x_{k+1}$  of  $x_k$  under the action of  $f$ . As in (21), the map is discontinuous at the point  $x = 0$  and defined as

$$f(0) = \begin{cases} 1 - \gamma & \text{for } x \rightarrow +0, \\ \gamma - 1 & \text{for } x \rightarrow -0. \end{cases} \quad (24)$$

By construction, the master map (23) is related to the cross-section  $D$ , and, therefore, is defined on the interval  $X = [-1, 1]$ . Its two fixed points  $e_l = x_1^* = -1$  and  $e_r = x_2^* = 1$  at the ends of the interval  $X$  correspond to the equilibrium points  $e_l$  and  $e_r$  of the flow system (1), respectively.

We will analyze attractors and their bifurcations in the master map (20) as a function of parameters  $\gamma$  and  $v$ . Our analysis can be summarized in the following theorem:

**Theorem 2:** 1. In the parameter region I (Fig. 5),

$$0 < \gamma < \gamma_h = 1, \quad (25)$$

the master map (23) has two stable fixed points  $e_r(x = 1)$  and  $e_l(x = -1)$  whose basins of attraction are the entire interval  $(-1, 1) \setminus (x = 0)$  [see Fig. 6(a)]. At  $\gamma_h = 1$ , corresponding to the homoclinic butterfly in the piecewise-smooth system (1), the singular point  $x = 0$  maps into itself such that two unstable points  $P_r(x = x_r)$  and  $P_l(x = x_l = -x_r)$  appear with increasing  $\gamma$  from  $\gamma_h = 1$ .

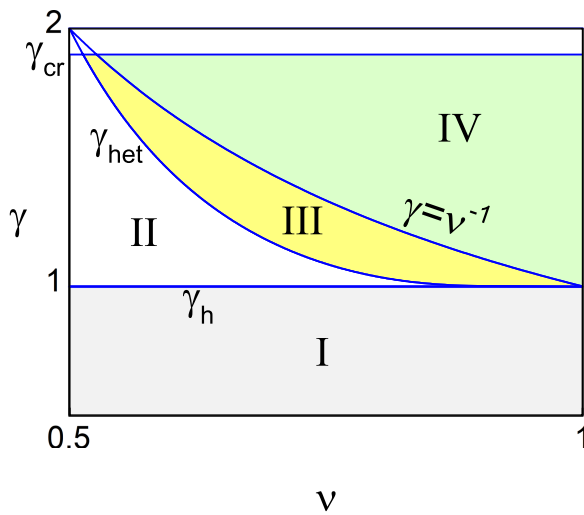


**FIG. 5.** The bifurcation diagram of the 1-D master map (23). Region I (gray) corresponds to globally stable fixed points  $e_r$  and  $e_l$ . Region II (white) corresponds to the dynamics similar to that of region I, except for the emergence of two unstable fixed points  $P_r$  and  $P_l$  and the invariant Cantor set of unstable trajectories that make the attraction basins of  $e_r$ ,  $e_l$  riddled. In region III (yellow), the map has three coexisting attractors: a strange chaotic attractor SA and two stable fixed points  $e_r$  and  $e_l$ . In region IV (green), the strange chaotic attractor is the only system's attractor. The horizontal line  $\gamma = \gamma_{cr}$  corresponds to the disappearance of the strange attractor due to the presence of stable sliding motions in the piecewise-smooth system (1).

2. In the parameter region II,

$$1 < \gamma < \gamma_{het}, \tag{26}$$

where  $\gamma_{het}$  is the root of the equation

$$\gamma - 2(\gamma - 1)^{1-\nu} = 0, \tag{27}$$

the stable fixed points  $e_r$  and  $e_l$  attract all trajectories from the interval  $(-1, 1)$ , besides the unstable fixed points  $P_r$  and  $P_l$ , and a nontrivial invariant Cantor set of unstable trajectories [see Fig. 6(b)].

3. In the parameter region III,

$$\gamma_{het} \leq \gamma < v^{-1}, \tag{28}$$

the map has a strange chaotic attractor (SA) which is contained inside the invariant interval  $X_{SA} = (1 - \gamma, \gamma - 1)$  [light green square in Fig. 6(c)]. This attractor is characterized by the property

$$f'(x) > 1, \quad x \in X_{SA} \tag{29}$$

and coexists with the two stable ( $e_r$  and  $e_l$ ) and two unstable ( $P_r$  and  $P_l$ ) fixed points [Fig. 6(c)].

4. In the parameter region IV,

$$v^{-1} \leq \gamma < \gamma_{cr}, \tag{30}$$

where  $\gamma_{cr}$  is defined in (22), the map has a unique (strange chaotic) attractor contained in the interval  $X_{SA}$  and whose basin of attraction is the entire interval  $X$  [Fig. 6(d)].

5. In the parameter region V (not marked in Fig. 5),

$$\gamma \geq \gamma_{cr}, \tag{31}$$

the attractor SA loses its chaotic property due to the emergence of stable sliding motions in the piecewise-smooth system (1) (see Theorem 1).

*Proof. Region I:*  $0 < \gamma < \gamma_h = 1$ .

The function  $f(x) > x \forall x \in (0, 1)$ ; therefore, each trajectory with  $x_0 \in (0, 1)$  approaches the endpoint of interval  $(0, 1)$ , fixed point  $e_r(x = 1)$ , whose local stability can also be verified as  $f'(1) = \gamma v < 1$  and  $f'(-1) = \gamma v < 1$  for  $\gamma < v^{-1}$ . A similar argument applies to the stability of the fixed point  $e_l(x = -1)$  which attracts all trajectories from the interval  $(-1, 0)$ .

*Region II:*  $1 < \gamma < \gamma_{het}$ .

Two unstable points  $P_r(x = x_r)$  and  $P_l(x = x_l = -x_r)$  appear after two disjoint parts of the graph  $f(x)$  merged together at the singularity point  $x = 0$  at  $\gamma = \gamma_h = 1$ , thereby exchanging the relative positions of their  $\bar{x}$  intercepts for  $\gamma > 1$  [compare Figs. 6(a) and 6(b)]. This justifies the left hand side of inequality (26).

The right-hand side of inequality (26) comes from the condition that the fixed point  $P_r(x = x_r)$  must be located lower than the  $\bar{x}$  intercept of the left leaf of the graph  $f(x)$  [see Fig. 6(b)]. This is true when  $x_r < \gamma - 1$ , where  $x_r = 1 - \gamma + \gamma x_r^\nu$ . Equating  $x_r$  and  $\gamma$  yields the

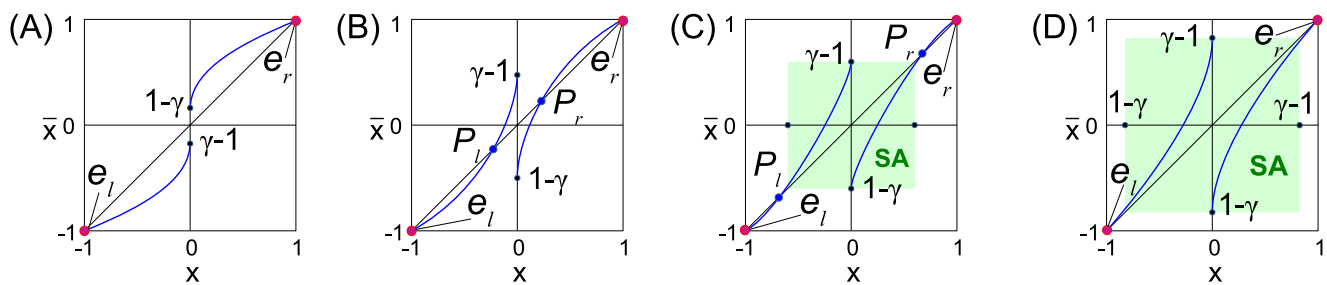


**FIG. 6.** The dependence of the master map's function  $f(x)$  (blue) on  $\gamma$ . (a)  $0 < \gamma < \gamma_h = 1$  (region I in Fig. 5): two stable fixed points  $e_l$  and  $e_r$ . (b)  $1 < \gamma < \gamma_{het}$  (region II): the emergence of unstable fixed points  $P_l(x = x_l)$  and  $P_r(x = x_r)$ . The fixed point  $P_r(x = x_r)$  [ $P_l(x = x_l)$ ] is below (above)  $\bar{x} = \gamma - 1$  [ $\bar{x} = 1 - \gamma$ ], which yields the Cantor set of unstable trajectories that are trapped inside the interval  $(x_l, x_r)$ . (c)  $\gamma_{het} \leq \gamma < v^{-1}$  (region III): The birth of a strange chaotic attractor SA which coexists with stable fixed points  $e_r$  and  $e_l$ . The unstable fixed point  $P_r(x = x_r)$  [ $P_l(x = x_l)$ ] lies above (below)  $\bar{x} = \gamma - 1$  [ $\bar{x} = 1 - \gamma$ ] making the interval  $(1 - \gamma, \gamma - 1)$  invariant for the attractor SA. (d)  $v^{-1} \leq \gamma < \gamma_{cr}$  (region IV): A unique (strange chaotic) attractor SA. The stable fixed points  $e_l$  and  $e_r$  have merged with the unstable points  $P_l$  and  $P_r$  and exchanged their stability, becoming unstable. The fixed points  $P_r$  and  $P_l$  lie outside of the interval  $[-1, 1]$  and are not shown.

condition (27) and critical value  $\gamma_{het}$ . In this case where  $\gamma - 1 > x_r$ , points from the interval  $(-x_0, x_0)$  where  $x_0$  is the preimage of the left fixed point  $x_l = 1 - \gamma + \gamma x_0^v$  leave the interval  $(x_l, x_r)$  and reach one of the stable fixed points  $e_r$  and  $e_l$ . What is left in the interval  $(x_l, x_r)$  after all preimages of the interval  $(-x_0, x_0)$  are removed is the Cantor set of unstable trajectories that are trapped inside the interval  $(x_l, x_r)$ .

*Region III:*  $\gamma_{het} \leq \gamma < v^{-1}$ .

As shown above, increasing  $\gamma$  such that  $\gamma > \gamma_{het}$ , moves the coordinate of the fixed point  $P_r(x = x_r)$  above the  $\bar{x}_1 = \gamma - 1$  intercept. This, together with the new location of the point  $P_l(x = x_l)$  below the other  $\bar{x}_2 = 1 - \gamma$  intercept, creates the trapping domain  $X_{SA} = (1 - \gamma, \gamma - 1)$  such that trajectories with  $x_0 \in X_{SA}$  cannot leave this interval, making it invariant [see Fig. 6(c)].

The derivative  $f'(x) = \gamma v |x|^{v-1}$  in the considered interval  $1/2 < v < 1$  [cf. assumption (8)] is a decreasing function of  $|x|$  with  $\lim_{|x| \rightarrow 0} f'(|x|) = \infty$ . Under these conditions,  $f'(x_l) > 1$  and  $f'(x_r) > 1$  (recall that the fixed points  $P_l$  and  $P_r$  are unstable). Therefore,  $f'(x) > 1$  for each point in the interval  $X_{lr} = \{|x| < x_r, x \neq 0\} = \{x_l < x < x_r, x \neq 0\}$ . The invariant interval  $X_{SA} = (1 - \gamma, \gamma - 1) \in X_{lr}$ , then  $f'(x) > 1$  for  $\forall x \in X_{SA}$  such that the trapping, invariant interval  $X_{SA}$  contains only unstable trajectories. These trajectories form a strange chaotic attractor and fill out the interval  $X_{SA}$ . The unstable fixed points  $P_l$  and  $P_r$  separate the attraction basins of the strange attractor SA and stable fixed points  $e_l$  and  $e_r$ . The right side of the inequality (28)  $\gamma < v^{-1}$  guarantees that  $x_r < 1$  and  $x_l > -1$  such that the points  $P_l$  and  $P_r$  do not merge with  $e_l$  and  $e_r$ .

*Region IV:*  $v^{-1} \leq \gamma < \gamma_{cr}$ .

At  $\gamma = v^{-1}$ , the fixed points  $P_r$  and  $e_r$  ( $P_l$  and  $e_l$ ) merge together as a result of a transcritical bifurcation and exchange their stability with further increase in  $\gamma > v^{-1}$ . The  $P_l$  and  $P_r$  leave the interval  $[-1, 1]$  and become irrelevant to the dynamics of the flow system (1). These changes preserve  $f'(x) > 1$  for  $\forall x \in X_{SA}$  and, therefore, do not affect the strange attractor SA, except that it becomes the only attractor of the map. This attractor preserves up to  $\gamma < \gamma_{cr}$  beyond which (in region V) the 1-D map does not adequately describe the flow system (1) due to the emergence of sliding motions which become a part of the system's attractor (see Theorem 1). □

**Remark 1:** The 1-D map (23) can be transformed into the standard 1-D Lorenz map<sup>9,11,12,15,61</sup>

$$\begin{aligned} \bar{\xi} &= -\mu + \xi^v \quad \text{for } \xi > 0, \\ \bar{\xi} &= \mu - |\xi|^v \quad \text{for } \xi < 0, \end{aligned} \tag{32}$$

by rescaling the variable  $x = k\xi$  with  $k = \gamma^{\frac{1}{1-v}}$  and introducing a new parameter  $\mu = (\gamma - 1)\gamma^{\frac{1}{1-v}}$ . However, there is a peculiar difference between the bifurcations of fixed points in the 1-D master map (23) and the standard 1-D Lorenz map (32). The parameter  $\mu$  in the standard 1-D Lorenz map is independent and can be changed monotonically from a negative to a positive value, thereby leading to a saddle-node bifurcation at which the fixed points  $P_r$  and  $e_r$  ( $P_l$  and  $e_l$ ) merge together and disappear. On the contrary, the parameter  $\mu$  in the 1-D map (32) obtained from the 1-D master map (23) is a function of parameters  $\gamma$  and  $v$  which has its maximum value at  $\gamma = 1/v$ . This value corresponds to the transcritical bifurcation at which the fixed points  $P_r$  and  $e_r$  ( $P_l$  and  $e_l$ ) merge together as a result of increasing  $\gamma$ , which reaches  $\gamma = 1/v$ . Further increasing  $\gamma$  decreases  $\mu$  and,

therefore, does not lead to the disappearance of the fixed points as in the standard 1-D map (32) with the independent parameter  $\mu$ , but rather induces their exchange of stability, rendering the fixed point  $e_r$  ( $e_l$ ) unstable. However, the fixed points  $e_r$  and  $e_l$  do not participate in the formation of the strange attractor and lie outside its invariant interval  $X_{SA}$  [see Fig. 6(d)]. As a result, this discrepancy between the fixed points of the 1-D master map (23) and the standard Lorenz map (32) with independent  $\mu$  is not important.

**Remark 2:** The curves  $\gamma = \gamma_{het}(v)$  and  $\gamma = v^{-1}$ , that define region III, intersect at  $v = 1/2$  and  $v = 1$ , thereby justifying our earlier assumption on the interval  $1/2 < v < 1$  where the strange attractor may exist, depending on  $\gamma$ . Note that  $\gamma_{cr} < 2$  for  $\lambda > 0$  since  $\gamma_{cr}|_{\lambda=0} = 2$  and the partial derivative  $(\gamma_{cr})_\lambda < 0$  indicating that  $\gamma_{cr}$  is a decreasing function of  $\lambda$ . This condition  $\gamma_{cr} < 2$  guarantees that the horizontal line  $\gamma = \gamma_{cr}$  lies below the  $\gamma = 2$  intercept of the curve  $\gamma = v^{-1}$ . Therefore, region IV  $v^{-1} \leq \gamma < \gamma_{cr}$ , which corresponds to the existence of the unique (strange) attractor of the map, remains nonempty for most values of  $1/2 < v < 1$ , except  $v$  close to  $1/2$  (see Fig. 5).

## V. DYNAMICS OF THE COMPLETE 2D MAP

Our goal is to connect the dynamics and bifurcations of the 1-D master map (23) to those of the complete 2D map  $F$  (20). It is important to notice that the  $y$  equation of the map (20):  $\bar{y} = g(x, y) \equiv r - 1 + r|x|^\alpha y$  is linear in  $y$ , with a discrete time-varying coefficient  $x$  which is governed by a trajectory of the master map (23). Due to the condition (22) on permissible values of parameter  $r$ , we can conclude that

$$r|x|^\alpha < \frac{1}{2\sqrt{2}} < 1, \quad \forall x \in [-1, 1]. \tag{33}$$

As a result, the  $y$  equation of (20) is contracting for  $\forall x \in [-1, 1]$  lying in the cross-section  $D$ . Thus, the  $y$  equation of (20) adds a stable direction to trajectories of the 1-D master map, thereby (i) preserving the stability of fixed points  $e_l$  and  $e_r$  when they are stable and (ii) turning unstable trajectories of the master map (20) into saddle trajectories of the 2D map (20). However, there are a few caveats associated with homoclinic and heteroclinic orbits that involve the discontinuity line  $l = (x = 0)$  where the 2D map is nonsmooth, and a careful proof of the above claim is needed. This leads to the following statement.

**Lemma 2:** 1. Stable fixed points  $e_l$  and  $e_r$  of the 1-D master map (20) in the parameter region  $0 < \gamma < v^{-1}$  yield stable fixed points  $e_l(x = -1, y = -1)$  and  $e_r = (x = 1, y = 1)$  of the 2D map (20).

2. Any unstable  $p$ -periodic (aperiodic) orbit of the 1-D master map, which is located inside the interval  $X = (1 - \gamma, \gamma - 1)$  and does not contain the singularity point  $x = 0$  induces a unique saddle  $p$ -periodic (aperiodic) orbit of the 2D map (20).

*Proof.* Due to the triangular form of the 2D map (20) where the  $x$ -equation drives the  $y$ -equation, each trajectory of the 1-D master map  $\{x_0, \dots, x_k, x_{k+1}, \dots\}$  generates a sequence of line segments  $\{L_0 = (x_k, y_k \in [-1, 1]), \dots, L_k, L_{k+1}, \dots\}$  in the 2D map. These line segments are often called leaves in a foliation on a Poincaré section of the Lorenz system.<sup>61</sup> For any  $x_k = f^k(x_0)$ ,  $y_k = g^k(x_0, y_0)$ ,  $k = 1, 2, \dots$ , the leaf  $L_k = \{x_k, y_k \in [-1, 1]\}$  is mapped into the leaf  $L_{k+1} = \{x_{k+1}, y_{k+1} \in [-1, 1]\}$ . In particular, the leaf  $L_1$ , corresponding to a fixed point of the 1-D master map, is invariant and maps

into itself. Let  $O_p = \{x_1^*, x_2^*, \dots, x_p^*, x_{p+1}^* = x_1^*\}$  be a  $p$ -periodic orbit of the 1-D master map which does not initiate from and never returns to the singularity point  $x = 0$ . This orbit induces the periodic leaves  $\{L_1, L_2, \dots, L_p, L_1\}$  such that any leaf  $L_j, j \in [1, p]$  is mapped into itself after  $p$  iterations. Substituting the values  $x_k$  from the orbit  $O_p$  into the  $y$  equation of 2D map (20), we obtain a sequence of linear maps  $y_{k+1} = g(x_k, y_k)$ , where we have switched to the conventional subscript notation for the next iterate. The composition of these maps results in the linear  $p$ th-iterate map of the leaf  $L_j$  into itself

$$y_{j+p} = Q_j + Q_0 y_j, j = \overline{1, p}, \tag{34}$$

where  $Q_0 = \prod_{k=1}^p r|x_k^*|^\alpha$  and  $Q_j = \text{const} \in L_j$ . The linear map (34) is contracting due to the inequality  $Q_0 < 1$  which follows from (33). Hence, this map has a unique stable fixed point  $y_j^* = \frac{Q_j}{1 - Q_0}$ . Connecting the sequence of stable fixed points  $y_1^*, y_2^*, \dots, y_p^*$  to the corresponding  $x_k$  values from the orbit  $O_p$ , we obtain a unique periodic orbit of the 2D map (20)  $\tilde{O}_p = \{(x_1^*, y_1^*), (x_2^*, y_2^*), \dots, (x_p^*, y_p^*)\}$ .

The eigenvalues of the Jacobian matrix of 2D map (20) are  $f'(x_k^*)$  and  $r|x_k^*|^\alpha$ , where  $x_k^*$  is governed by the periodic orbit  $\tilde{O}_p$ . Therefore, the Lyapunov exponents of the orbit  $\tilde{O}_p$  are

$$h_x = \frac{1}{p} \sum_{k=1}^p \ln |f'(x_k^*)|, \quad h_y = \frac{1}{p} \sum_{k=1}^p \ln r|x_k^*|^\alpha. \tag{35}$$

Due to the conditions (29) and (33), we obtain

$$h_x > 0, \quad h_y < 0 \quad \text{for } \gamma > 1. \tag{36}$$

This condition excludes the fixed points  $e_l$  and  $e_r$  of the 2D map, which are stable in the parameter region  $0 < \gamma < v^{-1}$ , with  $h_x < 0$  and  $h_y < 0$ . Thus,  $\tilde{O}_p$  is a unique saddle periodic orbit.

A similar argument applies to an unstable nonwandering, aperiodic trajectory  $O_\infty = \{x_1^*, x_2^*, \dots\}$  of the 1-D master map which does not contain the singularity point  $x = 0$  and yields a saddle aperiodic trajectory of the 2D map,  $\tilde{O}_\infty = \{(x_1^*, y_1^*), (x_2^*, y_2^*), \dots\}$ . Its Lyapunov exponents are

$$h_x = \lim_{n \rightarrow \infty} \frac{1}{n} \sum_{k=1}^n \ln |f'(x_k^*)|, \quad h_y = \lim_{n \rightarrow \infty} \frac{1}{n} \sum_{k=1}^n \ln r|x_k^*|^\alpha \tag{37}$$

whose lower and upper limits are bounded and satisfy the condition (36). Therefore,  $\tilde{O}_\infty$  is a unique orbit that corresponds to  $O_\infty$ .  $\square$

This lemma allows us to directly apply the statements of Theorem 2 to the dynamics of the 2D map. Before doing so and formulating these statements as a corollary, we shall discuss how the cross-section  $D$  transforms under the action of the 2D map  $F$ . As in the Poincaré return maps<sup>6-8</sup> of the original Lorenz system, the image  $FD$  of the cross-section  $D$  generated by our piecewise-smooth system (1) has two symmetric triangular shaped components  $F_1D_1$  and  $F_2D_2$  (see Fig. 7). The shape of the image  $F_1D_1$  is defined by the image of its boundary  $\partial D_1 = l \cup l_1 \cup l_+ \cup l_-$ , where  $l = (x = 0, y \in [-1, 1])$ ,  $l_1 = (x = 1, y \in [-1, 1])$ ,  $l_+ = (x \in (0, 1), y = 1)$ , and  $l_- = (x \in (0, 1), y = -1)$ . The image of the singularity line  $l$  is the point  $F_1l = M_1(1 - \gamma, 1 - r)$ ; the image of the invariant line  $l_1$  is the segment  $F_1l_1 = (x = 1, y \in [1 - 2r, 1])$ , where its upper boundary point is the fixed point  $e_r(x = 1, y = 1)$ . The image of the top line  $l_+$  is given in a parametric form  $F_1l_+ = (f(x), g(x, 1), x \in (0, 1])$ . Similarly, the image of the bottom line  $l_-$  is  $F_1l_- = (f(x), g(x, -1), x \in (0, 1])$ .

It is important to notice that the points  $M_1$  and  $M_2$  become cusp points if  $\alpha > v$  [cf. the imposed condition (8)]. This claim can be verified as follows. The upper bound of the triangular shaped component,  $F_1l_+$ , is described by a function  $\bar{y} = \kappa^+(\bar{x})$ ,  $\bar{x} \in (1 - \gamma, 1]$ , which is defined parametrically via  $\bar{x} = f(x)$ ,  $\bar{y} = g(x, 1)$ ,  $x \in (0, 1]$ .

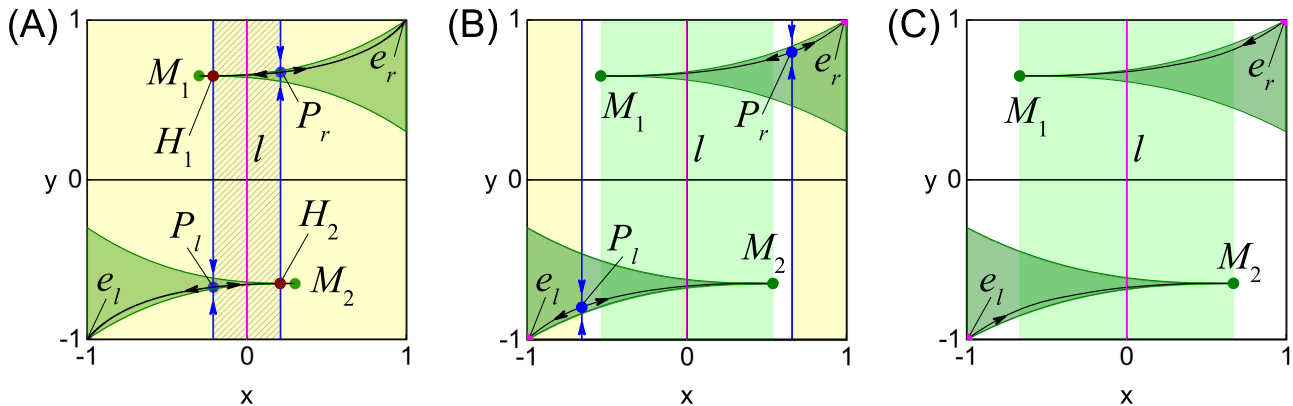


**FIG. 7.** The action of 2D map (20) as a function of parameter  $\gamma$ . The green triangular shaped areas are the images of cross-section  $D = (|x| \leq 1, |y| \leq 1)$ . Points  $M_1$  and  $M_2$  are the images of singularity line  $l$ . (a)  $1 < \gamma < \gamma_{net}$  (parameter region II in Fig. 5). The blue vertical (black curved) lines are the stable (unstable) manifolds of saddle fixed points  $P_l$  and  $P_r$ . Point  $H_1$  ( $H_2$ ) corresponds to a heteroclinic contour formed through transversal intersection between the stable manifold of  $P_l$  ( $P_r$ ) and the unstable manifold of  $P_r$  ( $P_l$ ). The shaded area contains the Cantor set of saddle trajectories. Attraction basins of stable fixed points  $e_r$  and  $e_l$  are marked in yellow. (b)  $\gamma_{net} \leq \gamma < v^{-1}$  (parameter region III). The strange attractor located in the invariant area (light green) coexists with two stable fixed points  $e_l$  and  $e_r$ . Two white vertical stripes are the attraction basin of SA. (c)  $v^{-1} \leq \gamma < \gamma_{or}$  (parameter region IV). The points  $P_r$  and  $P_l$  are no longer located inside the cross-section  $D$ . Fixed points  $e_l$  and  $e_r$  became saddles and made the strange attractor the only stable limit set of the map. The diagram from parameter region I is not shown.

Its derivative  $\kappa_{\bar{x}}^+ = \frac{g_x(x,1)}{f_x(x)} = \frac{r\alpha}{\gamma v} x^{\alpha-v}$  is positive for the region of interest  $x \in (0, 1]$ , which corresponds to the interval  $\bar{x} \in (1 - \gamma, 1]$  for its image. For  $\alpha > v$ , the derivative  $\kappa_{\bar{x}}^+$  approaches zero as  $x \rightarrow 0$ . Therefore, the graph of  $\kappa_{\bar{x}}^+$  has a horizontal tangent at  $x = 0$ , i.e., at the point  $M_1$ . Similarly, the graph of the lower bound,  $F_1 l_-$ , is defined by the function  $\bar{y} = \kappa^-(\bar{x})$ ,  $\bar{x} \in (1 - \gamma, 1]$  determined by  $\bar{x} = f(x)$ ,  $\bar{y} = g(x, -1)$ ,  $x \in (0, 1]$ . Its derivative  $\kappa_{\bar{x}}^- = -\kappa_{\bar{x}}^+$ , and, therefore, the graph of  $\kappa_{\bar{x}}^-$  also has a horizontal tangent at  $x = 0$ , corresponding to  $M_1$ . Therefore, the point  $M_1$  is a cusp point where the graphs of the upper and lower bounds merge together horizontally.

The shape of the image  $F_2 D_2$  is odd symmetric to  $F_1 D_1$  and consists of the point  $M_2(\gamma - 1, r - 1)$ , the segment  $(x = -1, y \in [-1, 2r - 1])$  containing the fixed point  $e_l(x = -1, y = -1)$ , and two lateral lines  $(f(x), g(x, 1), x \in [-1, 0))$  and  $(f(x), g(x, -1), x \in [-1, 0))$ . Due to the symmetry,  $M_2$  is also a cusp point for  $\alpha > v$ .

The evolution of the mutual arrangements of points  $M_1, M_2$ , and the singularity line  $l$  as a function of parameter  $\gamma$  controls the bifurcations and attractors of the 2D map as stated in the following corollary of Theorem 2 and Lemma 2.

**Corollary 1:** 1. In the parameter region I (25) (Fig. 5), the dynamics of the 2D map  $F$  is identical to that of the master map (23) except for the addition of the stable direction to the stable fixed points  $e_r(x = 1, y = 1)$  and  $e_l(x = -1, y = -1)$ . In terms of the images of Fig. 7,  $F_1 D_1 \subset D_1$  and  $F_2 D_2 \subset D_2$  such that the cusp point of the triangular image,  $M_1 (M_2)$ , also lies in  $F_1 D_1 (F_2 D_2)$  and does not reach the singularity line  $l$ . Subsequent images  $F_k \cdots F_1 D_1 (F_k \cdots F_2 D_2)$  preserve this arrangement and eventually shrink to the fixed point  $e_l (e_r)$ . For  $\gamma = 1$ , the cusp points  $M_1$  and  $M_2$  reach the line  $l$  to form the homoclinic butterfly in the piecewise-smooth system (1).

2. In the parameter region II (26), there appear two saddle points  $P_r(x_r, y_r), P_l(x_l, y_l)$ , where  $x_r$  and  $x_l$  are the coordinates of the unstable fixed points  $P_l$  and  $P_r$  of the 1-D master map [see Fig. 7(a)]. The 1-D stable manifold  $W_r^s$  of  $P_r$  is the invariant leaf  $L_r = (x = x_r, |y| \leq 1)$ . The  $x$  coordinate of point  $P_r$  is the stable fixed point of the 1-D master map corresponding to the leaf  $L_r$ , i.e.,  $y_r = \frac{1-r}{1-r|x_r|^\alpha}$ . The 1-D unstable manifold  $W_r^u$  of the point  $P_r$  has the edge points  $M_1$  and  $e_r$ . Symmetrically, the 1-D stable manifold  $W_l^s$  of  $P_l$  is the invariant leaf  $L_l = (x = x_l, |y| \leq 1)$ .

Due to the mutual arrangement of the points  $M_1, M_2$ , and stable manifolds  $W_l^s, W_r^s$  of saddle points  $P_l$  and  $P_r$ , there exist two heteroclinic points  $H_1 = W_l^s \cap W_r^u$  and  $H_2 = W_r^s \cap W_l^u$  such that the iterative points  $F^k H_1 \cup F^k H_2, k \in \mathbb{Z}$ , form a heteroclinic contour between two saddle points  $P_l$  and  $P_r$ . Induced by the dynamics of the 1-D master map, there exists the Cantor set of saddle trajectories which are located inside the domain bounded by the stable and unstable manifolds of saddle points  $P_l$  and  $P_r$  [inside the shaded area in Fig. 7(a)]. In this parameter region, the only attractors of the 2D map are stable fixed points  $e_r$  and  $e_l$ .

3. For  $\gamma = \gamma_{het}$ , the point  $M_1 (M_2)$  merges with  $H_1 (H_2)$ , causing a heteroclinic bifurcation. In terms of the piecewise-smooth system (1), this bifurcation occurs when the unstable manifold  $W_l^u (W_2^u)$  of saddle  $O$  whose image is point  $M_1 (M_2)$  falls on the stable manifold  $W_l^s (W_1^s)$  of the saddle limit cycle represented by the saddle point  $P_l (P_r)$ .

4. In the parameter region III (28), the point  $M_1 (M_2)$  lies to the right (left) from the stable manifold  $W_l^s (W_r^s)$  of saddles  $P_l (P_r)$  [see

Fig. 7(b)]. The strange attractor composed of only saddle trajectories is located in the region bounded by the points  $M_1$  and  $M_2$  in the  $x$  direction. The attraction basins of stable points  $e_l$  and  $e_r$  are bounded by the stable manifolds of saddles  $P_l$  and  $P_r$ , respectively.

5. In the parameter region IV (30), the strange attractor is a unique attracting set of the 2D map  $F$  due to a transcritical bifurcation transition similar to that of the 1-D master map when the saddle and stable points  $P_r, e_r (P_l, e_l, respectively)$  merge together at  $\gamma = v^{-1}$  and exchanged their stability. The points  $P_l$  and  $P_r$  left the cross-section  $D$  while edge fixed points  $e_r$  and  $e_l$  became saddle, making the strange attractor the only attractor [see Fig. 7(c)]. The chaoticity of this attractor is guaranteed by the presence of the positive Lyapunov exponent  $h_x$  due to (36). The singularity of this strange attractor is caused by the singular trajectories  $F^k M_1$  and  $F^k M_2, k \in \mathbb{Z}$ , which change the structure of the attractor when these trajectories return to the line  $l = W^s \cap D, F^k M_1 \in l, F^k M_2 \in l$ .

## VI. BACK TO THE FLOW DYNAMICS

According to Theorem 1, any trajectory of the piecewise-smooth system (1) reaches the absorbing domain  $G$ , making the cross-section  $D$  global. Therefore, the dynamics of the piecewise-smooth system (1) inside the absorbing domain  $G$  is fully defined by the trajectories of the 2D map  $F : D \rightarrow D$  (20). Given a discrete time orbit of the 2D map (20)  $K = \{ \dots, (x_k^*, y_k^*), (x_{k+1}^*, y_{k+1}^*), \dots, k = 0, 1, 2, \dots \}$ , connecting point  $(x_k^*, y_k^*)$  with point  $(x_{k+1}^*, y_{k+1}^*)$  by the corresponding systems'  $A_s$  and  $A_{r,l}$  solutions (3), (4), (5) yields the piece of the trajectory of the piecewise-smooth system (1) for any two neighbor iterative points of the discrete-time trajectory  $K$  of the 2D map.

As a result, bifurcation routes to the birth and disappearance of a strange attractor in the piecewise-smooth system (1) are identical to those of the 2D map (20), which are in turn determined by the 1-D master map (23). Therefore, we can recast the bifurcation diagram of the master map (Fig. 5) into the bifurcation parameters of the piecewise-smooth system (1),  $b = \gamma \exp \frac{3\pi\lambda}{2\omega}$  [cf. (19)] and  $v$ , where  $v$  is the same in both the flow system (1) and master map (see Fig. 8). To do so, we shall vary  $b$  by increasing  $\gamma$ , while keeping other parameters  $\alpha, \lambda, \delta$ , and  $\omega$  of the piecewise-smooth system (1) fixed. Here,  $\alpha > 1$  is chosen to satisfy the condition (8) and  $\delta < \delta_{cr}$  is chosen according to (11) in Theorem 1. Thus, Theorems 2, Lemma 2, and Corollary 1 can be summarized in terms of the piecewise-smooth system (1) as follows.

**Theorem 3:** A. In the parameter region (region I in Fig. 8),

$$0 < b < b_h = \exp \frac{3\pi\lambda}{2\omega}, \tag{38}$$

system (1) has two stable foci  $e_l$  and  $e_r$  that attract all system's trajectories, except for the saddle  $O_s$  and its stable 2D manifold  $W^s$  which separates the attraction basins [see Fig. 9(a) for the typical dynamics]. B. The surface

$$b_h = \exp \frac{3\pi\lambda}{2\omega} \tag{39}$$

corresponds to a homoclinic bifurcation of saddle  $O_s$  whose stable and unstable manifolds form two symmetrical homoclinic orbits (the homoclinic butterfly) [see Fig. 9(b)].

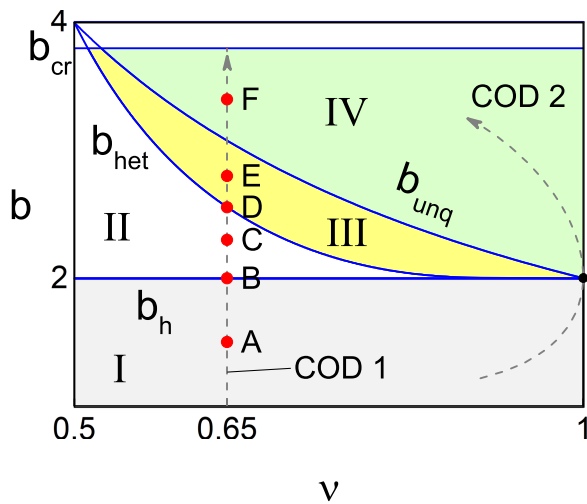


**FIG. 8.** The bifurcation diagram of Fig. 5 recast into the parameters of the piecewise-smooth system (1). Regions I–IV and their meaning are identical to those in Fig. 5. The bifurcation curves  $b_h$ ,  $b_{het}$ ,  $b_{unq}$ , and  $b_{cr}$  are plotted via the explicit formulas given in Theorem 3. The parameters are given in Fig. 9. The vertical dashed line  $\nu = 0.65$  exemplifies the main codimension-one bifurcation route COD1 to chaos. Points A, B, C, D, E, and F represent the typical dynamics in the corresponding regions depicted in Fig. 9. The curved dashed line indicates the route analogous to the route COD2 to chaos through the formation of the homoclinic butterfly with a zero saddle value in the Lorenz system.

C. In the parameter region (region II in Fig. 8),

$$b_h = \exp \frac{3\pi\lambda}{2\omega} < b < b_{het} = \gamma_{het} \exp \frac{3\pi\lambda}{2\omega}, \tag{40}$$

where  $\gamma_{het}$  is the inverse function of  $\nu = 1 + \frac{\ln 2 - \ln \gamma}{\ln(\gamma - 1)}$ , the stable foci  $e_r$  and  $e_l$  coexist with two symmetrical saddle cycles  $C_1$  and  $C_2$  which correspond to the saddle fixed points  $P_r = C_1 \cap D$  and  $P_l = C_2 \cap D$  of the 2D map. The unstable and stable manifolds of periodic orbits  $C_{1,2}$  intersect transversely, giving rise to a complicated Cantor set of saddle orbits [see Fig. 9(c) for the typical dynamics (the saddle cycles  $C_1$  and  $C_2$  are shown in Fig. 2)].

D. The surface

$$b_{het} = \gamma_{het} \exp \frac{3\pi\lambda}{2\omega} \tag{41}$$

corresponds to a heteroclinic bifurcation which yields the formation of two symmetrical heteroclinic contours composed of the unstable manifolds  $W^u$  of saddle point  $O_s$  that fall on the stable 2D manifolds of the saddle limit cycles  $C_1$  and  $C_2$  [see Fig. 9(d)].

E. In the parameter region (region III in Fig. 8),

$$b_{het} \leq b < b_{unq} = \nu^{-1} \exp \frac{3\pi\lambda}{2\omega}, \tag{42}$$

a strange chaotic Lorenz-type attractor which is born as the result of the heteroclinic bifurcation at  $b_{het}$  coexists with two stable foci  $e_l$  and  $e_r$  [see Fig. 9(E)].

E–F. The surface

$$b_{unq} = \nu^{-1} \exp \frac{3\pi\lambda}{2\omega} \tag{43}$$

corresponds to a subcritical Andronov-Hopf-like bifurcation<sup>62</sup> when the saddle periodic orbit  $C_1$  ( $C_2$ ) shrinks to the stable focus  $e_r$  ( $e_l$ ) and disappears, rendering  $e_r$  ( $e_l$ ) a saddle-focus.

F. In the parameter region (region IV in Fig. 8)

$$\nu^{-1} \exp \frac{3\pi\lambda}{2\omega} \leq b < 2\sqrt{1 + \frac{\lambda^2}{\omega^2}} \exp \left\{ \frac{\lambda}{\omega} \left( \arctan \frac{\omega}{\lambda} + \pi \right) \right\}, \tag{44}$$

the strange Lorenz-type attractor becomes a unique attractor of the piecewise-smooth system (1) [see Fig. 9(f)].

G. The surface

$$b = b_{cr} = 2\sqrt{1 + \frac{\lambda^2}{\omega^2}} \exp \left\{ \frac{\lambda}{\omega} \left( \arctan \frac{\omega}{\lambda} + \pi \right) \right\} \tag{45}$$

corresponds to the emergence of stable sliding motions inside the attractor which destroy its chaoticity.

*Proof.* The proof of claims A–G directly follows from the corresponding claims of Theorem 2, Lemma 2, and Corollary 1. However, one point in claim E–F which states that the transcritical bifurcation in the 2D map (20) induces a subcritical Andronov-Hopf-like bifurcation in the piecewise-smooth system (1) requires a clarification. Recall that this transcritical bifurcation occurs in the 2D map (20) when the fixed points  $P_r$  and  $e_r$  ( $P_l$  and  $e_l$ ) merge together and exchange their stability such that the point  $P_r$  ( $P_l$ ) becomes stable and leaves the cross-section  $D = (|x| \leq 1, |y| \leq 1)$ . However, this bifurcation transition does not fully translate into bifurcations in the piecewise-smooth system (1) as piecewise-smooth systems can exhibit transitions not possible in smooth systems, including boundary equilibrium bifurcations.<sup>38,63</sup> More specifically, before the bifurcation, in the parameter region III, the fixed point  $P_r$  ( $P_l$ ) of the 2D map represents a saddle limit cycle  $C_1$  ( $C_2$ ), while the fixed point  $e_r$  ( $e_l$ ) of the 2D map corresponds a stable focus  $e_r$  ( $e_l$ ) in (1). At  $b = b_{unq}$ , the stable focus undergoes a subcritical Andronov-Hopf-like bifurcation so that the saddle limit cycle shrinks into the stable focus. According to the transcritical transition in the 2D map, one would expect that the fixed point and the limit cycle would exchange their stability, making the stable focus a saddle-focus and giving birth to a small-amplitude stable limit cycle. However, this is not the case since the prototype of this limit cycle, the point  $P_l$  lies outside the cross-section  $D$  such that it is not defined by the flow of system (1) and, therefore, is irrelevant to the dynamics of the piecewise-smooth system (1) and should be ignored. This results in the bifurcation transition described in claim E–F that the saddle limit cycle  $C_1$  ( $C_2$ ) merges into the stable focus point  $e_r$  ( $e_l$ ) and disappears, rendering  $e_r$  ( $e_l$ ) a saddle-focus.  $\square$

Figure 8 indicates the bifurcation route COD1 in the piecewise-smooth system (1) which is identical to the main route COD1 to the birth of the Lorenz attractor in the original Lorenz system. It is worth noticing that the codimension-two route COD2 in the Lorenz model can be realized in the piecewise-smooth system as indicated in Fig. 8. Here, one has to follow the dashed curve and change two parameters  $\nu$  and  $b$  simultaneously as  $\nu$  may only be equal to 1 at the bifurcation point (see Remark 2). Note that the piecewise-smooth system

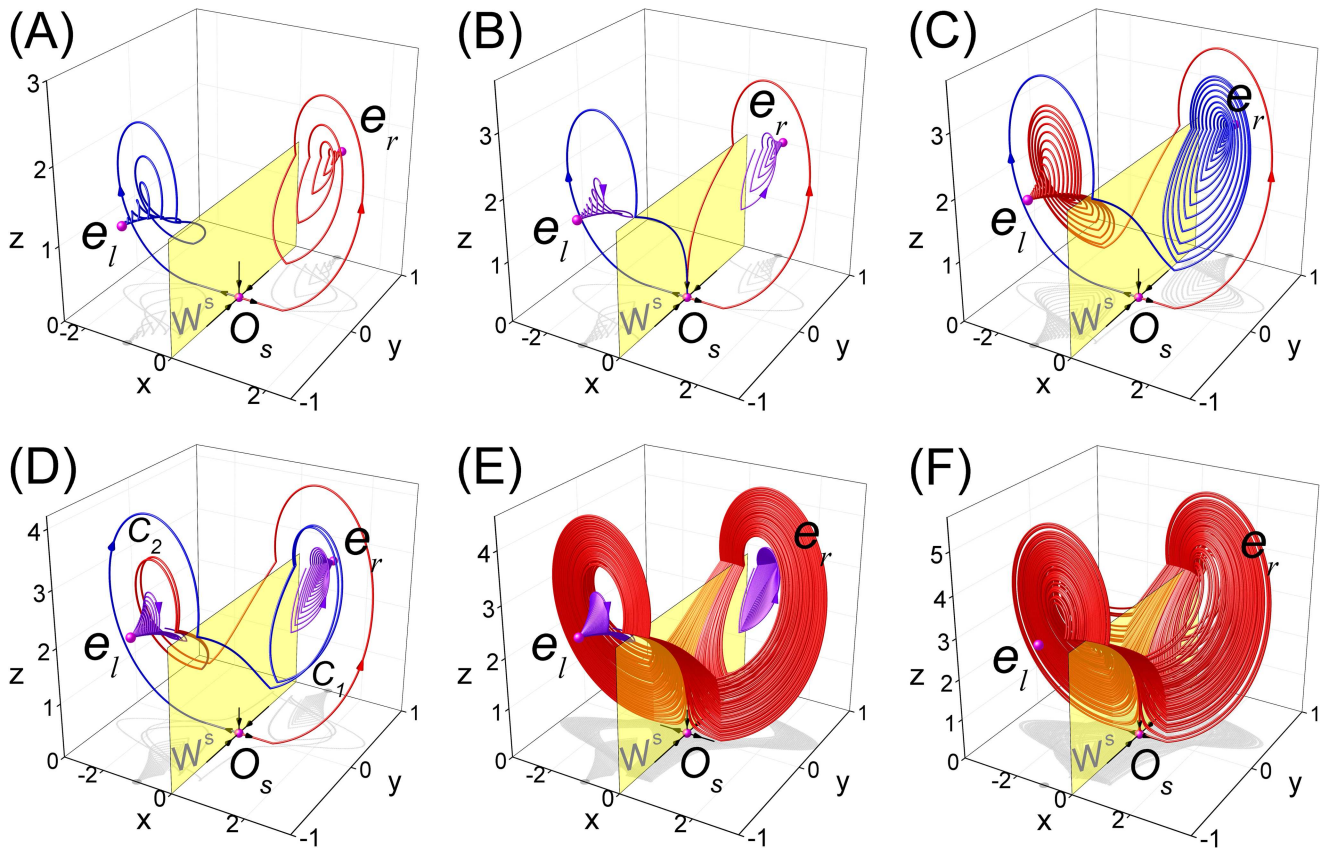


**FIG. 9.** The dynamics of the piecewise-smooth system (1) as a function of parameter  $b$ . Subplots (a), (b), (c), (d), (e), and (f) demonstrate the dynamics that correspond to points (a), (b), (c), (d), (e), and (f) in the bifurcation diagram of Fig. 8, respectively. (a)  $b = 1.5$ . Two stable foci  $e_l$  and  $e_r$  (pink circles) attract the unstable manifolds (red and blue) of saddle  $O_s$ . (b)  $b = b_h = 2$ . The homoclinic butterfly. The unstable manifolds (red and blue) return to saddle  $O_s$ , forming two symmetric homoclinic orbits. The nonsmooth shape of the homoclinic orbits is due to the piecewise-smooth nature of system (1). (c)  $b = 2.3$ . Stable foci  $e_r$  and  $e_l$  coexist with two symmetrical saddle cycles  $C_1$  and  $C_2$  (not shown). (d)  $b = b_{het} = 2.557$ . The heteroclinic bifurcation. It involves the formation of two heteroclinic orbits of saddle  $O_s$  that connect to two symmetric saddle limit cycles  $C_1$  and  $C_2$ . The Lorenz-type strange attractor is born at this bifurcation (not shown). (e)  $b = 2.8$ . The strange attractor (red) coexists with stable foci  $e_l$  and  $e_r$ . The purple trajectories are attracted by  $e_l$  and  $e_r$ . (f)  $b = 3.4$ . The strange attractor is the only attractor of system (1). Other parameters are  $\alpha = 2$ ,  $\nu = 0.65$ ,  $\lambda = 0.294$ ,  $\omega = 2$ , and  $\delta = 0.588$ .

allowed us to explicitly indicate the system’s parameters that yield the complete cascade of bifurcations leading to chaos, including the homoclinic butterfly (point B) and the heteroclinic bifurcation (point C) (also see Fig. 9). These analytical tasks are out of reach for the Lorenz system.

Recall that the 2D map (20), which yields the bifurcation diagram of Fig. 8, is constructed under the condition (22) on the system’s parameters that guarantees that the attractors of the piecewise-smooth system (1) do not contain sliding motions. Although it has a different origin, this restriction can be viewed as an analog of the foliation condition in the geometric Lorenz model which guarantees that the chaotic attractor is described by the one-dimensional Lorenz map.<sup>15</sup> Failure of the foliation condition<sup>16,64,65</sup> in the original Lorenz system leads to the appearance of Smale horseshoes in the Lorenz map and the transformation of the chaotic Lorenz attractor into a quasiattractor that contains stable periodic orbits.

Similarly, failure of the condition (22) for  $b \geq b_{cr}$  leads to the disappearance of the singular hyperbolic Lorenz-type attractor due to the emergence of the stable sliding motions. A remarkable feature of the piecewise-smooth system (1) is that it can offer a rigorous description for the structure and bifurcations of the system’s quasiattractors which contain stable sliding motions in the parameter range  $b \geq b_{cr}$ . This can be done by refining the construction of the Poincaré return map (20), which should account for the trajectories of focus systems  $A_r$  and  $A_l$  that reach the stable sliding regions and eventually return to the cross-section  $D$ . The locations of the points at which these trajectories land on the cross-section  $D$  representing the next iterate of the Poincaré return map can be rigorously identified via the linear system (10). In terms of the explicit 1-D master map, this refinement due to the stable sliding motions will induce two symmetric flat fragments in the graph of function  $f(x)$  which lead to the collapse of the corresponding  $x$  intervals into two points as opposed



to the appearance of hooked horseshoes in the geometric Lorenz map due to the failed foliation condition.<sup>65</sup> The detailed analysis of the emerging quasiattractor is beyond the scope of this work and will be reported elsewhere.

## VII. CONCLUSIONS

In this paper, we have proposed a geometrical approach to building a piecewise-smooth ODE model which switches between three-dimensional linear ODE systems and generates a chaotic attractor whose existence can be rigorously proven. We have chosen the Lorenz attractor as a motivating example to reproduce its structure and the sequence of bifurcations that leads to its formation and disappearance, but in a more analytically tractable system than the original nonintegrable Lorenz system.

The use of our piecewise-smooth ODE model has allowed for characterizing this sequence of bifurcations rigorously and expressing the corresponding bifurcation curves explicitly via the system's parameters. In particular, we have analytically calculated a bifurcation curve that corresponds to the formation of homoclinic orbits of a saddle, known as homoclinic butterflies. We have rigorously proved that the Lorenz-type attractor in our model is born as a result of a bifurcation of two heteroclinic orbits connecting the saddle fixed point and two symmetrical saddle periodic orbits, as in the original Lorenz system. Similarly, we have demonstrated that the attractor can be a unique attracting set or can coexist with two stable equilibria. Remarkably, our system has reproduced the well-known cascade of bifurcations that gives birth to the Lorenz attractor in the Lorenz system rather precisely. We have used an explicit Poincaré return map and analytically calculated Lyapunov exponents for the system's trajectories to prove the existence of the chaotic Lorenz-type attractor in our piecewise-smooth system. Notably, a similar task of proving the existence of the original Lorenz attractor turned out to be a long-term existing challenge that had been resolved only recently.<sup>2,3,26</sup> In this regard, our piecewise-smooth ODE model in which a strange hyperbolic attractor is glued from graphs of closed-form solutions offers a simpler approach to rigorously proving the existence of a chaotic attractor. However, this novel approach comes with the price of a synthetically designed dynamical system and its increased structural complexity due to necessary switching between its three linear components.

Due to its construction, the main properties of our Lorenz-type attractor are analytically tractable, including its hyperbolicity. As a result, our piecewise-smooth ODE system along with its triangular-form, explicit Poincaré map may allow for studying its ergodic properties and constructing its natural invariant measure similarly to the classical ergodic theory studies of the Lorenz system.<sup>66–68</sup>

Our geometrical approach is not limited to three-dimensional systems and can be extended to reproduce the dynamics of high-dimensional versions of the Lorenz system.<sup>69</sup> A straightforward extension of the model and our analysis involves the replacement of the  $y$  scalar variable with a vector. Our geometrical approach of building an analytically tractable piecewise-smooth dynamical system with a predefined chaotic attractor can also be applied to reproduce and rigorously prove bifurcation properties of chaotic attractors which are similar to their counterparts in the classical nonswitching dynamical systems, including the Chua and Rössler attractors whose

quantitative analysis has been largely limited to numerical simulations. The Chua system is a classical example of a three-dimensional piecewise-linear system which contains a saddle-focus and exhibits Shilnikov chaos. While the use of a piecewise-linear function as a nonlinearity in the Chua system simplifies the system's analysis, a rigorous, computer-free study of the system's attractor is impaired by the inability to derive closed-form solutions and explicitly assess their stability.<sup>40</sup> In light of this, constructing a piecewise-smooth dynamical system similar to the one proposed in this paper which switches between three linear subsystems (as the Chua system also has three equilibria) may offer a way of synthesizing and rigorously studying a chaotic attractor which resembles the Chua attractor.

When used as a unit composing a dynamical network, our analytically tractable model may provide a rigorous basis for understanding complex cooperative dynamics of coupled systems. These include evolving<sup>70</sup> and stochastically switching dynamical networks<sup>71,72</sup> which exhibit highly-nontrivial dynamics such as the emergence of ghost attractors<sup>73</sup> and unexpected regions of intermediate switching, called windows of opportunity,<sup>74</sup> in which synchronization in a switching network of chaotic oscillators becomes stable even though it is unstable in the averaged/fast switching network. While the emergence of windows of opportunity was analytically addressed for networks of coupled chaotic maps,<sup>75,76</sup> its rigorous proof for networks of coupled ODE systems calls for future studies. In light of this, the use of our piecewise-smooth ODE model with closed-form solutions and Lyapunov exponents may become a key to rigorously solving this stability problem.

## ACKNOWLEDGMENTS

This work was supported by the RFBR under Grant Nos. 18-01-00556 (to V.N.B. and N.V.B.) and 18-31-20052 (to N.V.B.), the RSF (numerics) under Grant No. 19-12-00367 (to V.N.B. and N.V.B.), and the National Science Foundation (NSF) (USA) under Grant Nos. DMS-1616345 and DMS-1909924 (to I.V.B.).

## REFERENCES

- <sup>1</sup>E. Lorenz, *J. Atmos. Sci.* **20**, 130 (1963).
- <sup>2</sup>W. Tucker, *C. R. l'Acad. Sci. Ser. I* **328**, 1197 (1999).
- <sup>3</sup>I. Stewart, *Nature* **406**, 948–949 (2000).
- <sup>4</sup>D. Ruelle and F. Takens, *Commun. Math. Phys.* **20**, 167 (1971).
- <sup>5</sup>V. N. Belykh, *Great Russian Encyclopedia* (Great Russian Encyclopedia, Moscow, 2016), Vol. 31, p. 285 (in Russian).
- <sup>6</sup>J. Guckenheimer, "A strange, strange attractor," *The Hopf Bifurcation and Its Applications*, Applied Mathematical Sciences (Springer, New York, NY, 1976), pp. 368–381.
- <sup>7</sup>V. S. Afraimovich, V. V. Bykov, and L. P. Shilnikov, *Akademiia Nauk SSSR Dokl.* **234**, 336 (1977).
- <sup>8</sup>V. S. Afraimovich, V. V. Bykov, and L. P. Shilnikov, *Trans. Mosc. Math. Soc.* **44**, 153 (1982).
- <sup>9</sup>J. Guckenheimer and P. Holmes, *Nonlinear Oscillations, Dynamical Systems, and Bifurcations of Vector Fields* (Springer, 1983).
- <sup>10</sup>R. F. Williams, *Inst. Hautes Etudes Sci. Publ. Math.* **50**, 73 (1979).
- <sup>11</sup>C. Robinson, *Nonlinearity* **2**, 495–518 (1989).
- <sup>12</sup>C. Robinson, *SIAM J. Math. Anal.* **23**, 1255–1268 (1992).
- <sup>13</sup>M. R. Rychlik, *Ergodic Theory Dyn. Syst.* **10**(4), 793 (1990).
- <sup>14</sup>C. A. Morales, M. J. Pacifico, and E. R. Pujals, *Proc. AMS* **127**, 3393–3401 (1999).
- <sup>15</sup>C. Sparrow, *The Lorenz Equations: Bifurcations, Chaos and Strange Attractors* (Springer, 1982).

- <sup>16</sup>V. V. Bykov and A. L. Shilnikov, *Selecta Math. Sov.* **11**, 375–382 (1992).
- <sup>17</sup>R. Barrio, A. Shilnikov, and L. Shilnikov, *Int. J. Bifurcat. Chaos* **22**, 1230016 (2012).
- <sup>18</sup>E. J. Doedel, B. Krauskopf, and H. M. Osinga, *Nonlinearity* **19**, 2947 (2006).
- <sup>19</sup>E. J. Doedel, B. Krauskopf, and H. M. Osinga, *Nonlinearity* **28**, R113 (2015).
- <sup>20</sup>D. Viswanath, *Nonlinearity* **16**, 1035 (2003).
- <sup>21</sup>B. Hassard, J. Zhang, S. Hastings, and W. Troy, *Appl. Math. Lett.* **7**, 79 (1994).
- <sup>22</sup>Z. Galias and P. Zgliczyński, *Physica D* **115**, 165 (1998).
- <sup>23</sup>M. Breden and J.-P. Lessard, *Discrete Cont. Dyn. Syst. B* **23**, 2825 (2018).
- <sup>24</sup>K. Mischaikow and M. Mrozek, *Bull. Am. Math. Soc.* **32**, 66 (1995).
- <sup>25</sup>B. Hassard and J. Zhang, *SIAM J. Math. Anal.* **25**, 179 (1994).
- <sup>26</sup>I. I. Ovsyannikov and D. V. Turaev, *Nonlinearity* **30**, 115 (2017).
- <sup>27</sup>L. Shilnikov, *Uspehi Mat. Nauk* **36**, 240 (1981).
- <sup>28</sup>A. N. Wittig, “Rigorous high-precision enclosures of fixed points and their invariant manifolds,” Ph.D. thesis (Michigan State University, 2012).
- <sup>29</sup>V. Belykh, *Differ. Equ.* **20**, 1184 (1984).
- <sup>30</sup>A. A. Andronov, A. A. Vitt, and S. E. Khaikin, *Theory of Oscillations* (Fizmatgiz, Moscow, 1959).
- <sup>31</sup>A. R. Champneys and M. di Bernardo, *Scholarpedia* **3**, 4041 (2008).
- <sup>32</sup>Z. T. Zhusubaliyev and E. Mosekilde, *Bifurcations and Chaos in Piecewise-Smooth Dynamical Systems*, World Scientific Series on Nonlinear Science Series A (World Scientific, 2003), Vol. 44.
- <sup>33</sup>A. C. Luo and L. Chen, *Chaos Soliton. Fract.* **24**, 567 (2005).
- <sup>34</sup>N. Levinson, *Ann. Math. Second Ser.* **50**, 127 (1949).
- <sup>35</sup>M. L. Cartwright and J. E. Littlewood, *J. Lond. Math. Soc.* **20**, 180 (1945).
- <sup>36</sup>A. S. Elwakil, S. Ozoguz, and M. P. Kennedy, *IEEE Trans. Circuits Syst. I* **49**, 4 (2002).
- <sup>37</sup>C. Lia, J. C. Sprott, and W. Thio, *Phys. Lett. A* **379**, 888–893 (2015).
- <sup>38</sup>M. di Bernardo, C. Budd, A. Champneys, and P. Kowalczyk, *Piecewise-smooth Dynamical Systems. Theory and Applications* (Springer, 2007).
- <sup>39</sup>N. Gubar, *J. Appl. Math. Mech.* **25**(6), 1011–1023 (1961).
- <sup>40</sup>T. Matsumoto, L. Chua, and M. Komoro, *Physica D* **24**, 97 (1987).
- <sup>41</sup>M. di Bernardo, M. I. Feigin, S. J. Hogan, and M. E. Homer, *Chaos Soliton. Fract.* **10**, 1881 (1999).
- <sup>42</sup>D. J. Simpson, S. J. Hogan, and R. Kuske, *SIAM J. Appl. Dyn. Syst.* **12**, 533 (2013).
- <sup>43</sup>I. Belykh, R. Jeter, and V. Belykh, *Sci. Adv.* **3**, e1701512 (2017).
- <sup>44</sup>J. H. Macdonald, *Proc. R. Soc. Lond. A* **465**, 1055 (2008).
- <sup>45</sup>I. V. Belykh, R. Jeter, and V. N. Belykh, *Chaos* **26**, 116314 (2016).
- <sup>46</sup>R. N. Madan, *Chua’s Circuit: A Paradigm for Chaos* (World Scientific Publishing, 1993).
- <sup>47</sup>O. E. Rössler, *Phys. Lett. A* **57**, 397 (1976).
- <sup>48</sup>C. A. Morales, M. J. Pacifico, and E. R. Pujals, *C. R. l’Acad. Sci. Ser. I* **326**, 81 (1998).
- <sup>49</sup>D. V. Turaev and L. P. Shilnikov, *Mat. Sb.* **189**, 137–160 (1998).
- <sup>50</sup>E. A. Sataev, *Mat. Sb.* **200**, 37 (2009).
- <sup>51</sup>*Handbook of Dynamical Systems*, edited by B. Hasselblatt and A. Katok (Elsevier, 2006).
- <sup>52</sup>C. Robinson, *Dynamical Systems: Stability, Symbolic Dynamics, and Chaos* (CRC Press, 1998).
- <sup>53</sup>V. Belykh, I. Belykh, and E. Mosekilde, *Int. J. Bifurcat. Chaos* **15**, 3567 (2005).
- <sup>54</sup>S. P. Kuznetsov, *Chaos* **19**, 013114 (2009).
- <sup>55</sup>S. P. Kuznetsov, *Phys. Rev. Lett.* **95**, 144101 (2005).
- <sup>56</sup>S. P. Kuznetsov, *Hyperbolic Chaos* (Springer, 2012).
- <sup>57</sup>V. N. Belykh and I. Belykh, *Scholarpedia* **6**, 5545 (2011).
- <sup>58</sup>V. Afraimovich, N. Chernov, and E. Sataev, *Chaos* **5**, 238 (1995).
- <sup>59</sup>M. V. Shashkov and D. V. Turaev, *J. Nonlinear Sci.* **9**, 525–573 (1999).
- <sup>60</sup>A. Filippov, *Differential Equations with Discontinuous Right-hand Sides* (Kluwer Academic Press, 1988).
- <sup>61</sup>L. P. Shilnikov, A. L. Shilnikov, D. V. Turaev, and L. Chua, *Qualitative Theory in Nonlinear Dynamics. Part II* (World Scientific, 2001).
- <sup>62</sup>Limit cycles in piecewise-smooth dynamical systems can be born or can disappear in ways fundamentally different from the smooth systems.<sup>38</sup> For example, see Ref. 63 for a compendium of 20 different geometric mechanisms by which limit cycles are created locally in a two-dimensional piecewise-smooth system of ODEs. The bifurcations determining these mechanisms include boundary equilibrium bifurcations and limit cycles created from folds and are often called Andronov-Hopf-like (or simply Hopf-like) bifurcations as in each case a fixed point changes stability and produces a limit cycle. We also follow this name convention in this paper.
- <sup>63</sup>D. Simpson, *Phys. Lett. A* **382**, 2439 (2018).
- <sup>64</sup>A. L. Shilnikov, *Physica D* **62**, 338 (1993).
- <sup>65</sup>J. L. Creaser, B. Krauskopf, and H. M. Osinga, *SIAM J. Appl. Dyn. Syst.* **16**, 2127 (2017).
- <sup>66</sup>L. Bunimovich and Y. G. Sinai, “Stochasticity of the attractor in the Lorenz model,” in *Nonlinear Waves*, edited by A. V. Gaponov-Grekhov and M. I. Rabinovich (Nauka, Moscow, 1979), pp. 212–226.
- <sup>67</sup>J. G. Sinai and E. B. Vul, *Physica D* **2**, 3 (1981).
- <sup>68</sup>E. A. Sataev, *Mat. Sb.* **201**, 419 (2010).
- <sup>69</sup>C. Bonatti, A. Pumariño, and M. Viana, in *Equadiff 99* (World Scientific, 2000), 2 Vols., pp. 39–44.
- <sup>70</sup>I. Belykh, M. di Bernardo, J. Kurths, and M. Porfiri, *Physica D* **267**, 1 (2014).
- <sup>71</sup>M. Hasler, V. Belykh, and I. Belykh, *SIAM J. Appl. Dyn. Syst.* **12**, 1031 (2013).
- <sup>72</sup>N. Barabash and V. Belykh, *Radiophys. Quant. Electron.* **60**, 761 (2018).
- <sup>73</sup>I. Belykh, V. Belykh, R. Jeter, and M. Hasler, *Eur. Phys. J. Spec. Top.* **222**, 2497 (2013).
- <sup>74</sup>R. Jeter and I. Belykh, *IEEE Trans. Circuits Syst. I* **62**, 1260 (2015).
- <sup>75</sup>O. Golovneva, R. Jeter, I. Belykh, and M. Porfiri, *Physica D* **340**, 1 (2017).
- <sup>76</sup>R. Jeter, M. Porfiri, and I. Belykh, *Chaos* **28**, 071104 (2018).